PA 1032918

THE UNITED STATES OF AMERICA

TO ALL TO WHOM THESE PRESENTS SHALL COME:

UNITED STATES DEPARTMENT OF COMMERCE

United States Patent and Trademark Office

July 02, 2003

THIS IS TO CERTIFY THAT ANNEXED HERETO IS A TRUE COPY FROM THE RECORDS OF THE UNITED STATES PATENT AND TRADEMARK OFFICE OF THOSE PAPERS OF THE BELOW IDENTIFIED PATENT APPLICATION THAT MET THE REQUIREMENTS TO BE GRANTED A FILING DATE UNDER 35 USC 111.

APPLICATION NUMBER: *60/392,489*
FILING DATE: *June 28, 2002*

PRIORITY DOCUMENT
SUBMITTED OR TRANSMITTED IN
COMPLIANCE WITH
RULE 17.1(a) OR (b)

By Authority of the
COMMISSIONER OF PATENTS AND TRADEMARKS

P. R. GRANT
Certifying Officer

07-01-02 A/P

Please type a plus sign (+) inside this box → [+]

PTO/SB/16 (8-00)
Approved for use through 10/31/2002. OMB 0651-0032
U.S. Patent and Trademark Office; U.S. DEPARTMENT OF COMMERCE

Under the Paperwork Reduction Act of 1995, no persons are required to respond to a collection of information unless it displays a valid OMB control number.

PROVISIONAL APPLICATION FOR PATENT COVER SHEET

This is a request for filing a PROVISIONAL APPLICATION FOR PATENT under 37 CFR 1.53(c).

JC913 U.S. PTO 60/387487

INVENTOR(S)

Given Name (first and middle [if any])	Family Name or Surname	Residence (City and either State or Foreign Country)
Erez N. RIBAK	Hasman	Hadera, Israel

☐ *Additional inventors are being named on the ___ separately numbered sheets attached hereto*

TITLE OF THE INVENTION (280 characters max)

Pancharatnam-Berry Phase Optical Elements with Suwavelength Gratings

Direct all correspondence to: **CORRESPONDENCE ADDRESS**

☑ Customer Number 23521

OR *Type Customer Number here*

Please Customer Number Bar Code Label Here 23521

PATENT TRADEMARK OFFICE

☐ Firm or Individual Name					
Address					
Address					
City		State		ZIP	
Country		Telephone		Fax	207-767-5324

ENCLOSED APPLICATION PARTS (check all that apply)

☑ Specification *Number of Pages* 39

☑ Drawing(s) *Number of Sheets* 17

☐ Application Data Sheet. See 37 CFR 1.76

☐ CD(s), Number

☐ Other (specify)

METHOD OF PAYMENT OF FILING FEES FOR THIS PROVISIONAL APPLICATION FOR PATENT

☑ Applicant claims small entity status. See 37 CFR 1.27.

☐ A check or money order is enclosed to cover the filing fees

☑ The Commissioner is hereby authorized to charge filing fees or credit any overpayment to Deposit Account Number: 501392

☑ Payment by credit card. Form PTO-2038 is attached.

FILING FEE AMOUNT ($): **$80.00**

The invention was made by an agency of the United States Government or under a contract with an agency of the United States Government.

☑ No.

☐ Yes, the name of the U S. Government agency and the Government contract number are: _____

Respectfully submitted,

SIGNATURE Shalom W.

Date June 27, 2002

TYPED or PRINTED NAME Shalom Wertsberger

REGISTRATION NO (if appropriate) 43,359

Docket Number: 0226USP-Hasman

TELEPHONE (207) 799-9733

Express Mail # EJ676543683US

USE ONLY FOR FILING A PROVISIONAL APPLICATION FOR PATENT

This collection of information is required by 37 CFR 1.51. The information is used by the public to file (and by the PTO to process) a provisional application. Confidentiality is governed by 35 USC 122 and 37 CFR 1.14. This collection is estimated to take 8 hours to complete, including gathering, preparing and submitting the complete provisional application to the PTO. Time will vary according to the individual case.

Certificate under 37 CFR 1.10 of Mailing by "Express Mail"

EJ676543683US
"Express Mail" label number

June 28, 2002
Date of Deposit

I hereby certify that this correspondence is being deposited with the United States Postal Service "Express Mail Post Office to Addressee" service under 37 CFR 1.10 on the date indicated below and is addressed to the Commissioner for Patents, Washington, D.C. 20231

Signature of person mailing correspondence

Shalom Wertsberger Reg. No. 43,359
Typed or printed name of person mailing correspondence

Docket: 0226USP-Hasman **Application #:** _____

Inventor: Erez Hasman **Filed on:** _____

Title: Pancharatnam-Berry Phase Optical Elements with Suwavelength Gratings

This corespondence contains:

1 page transmittal sheet
39 pages of written specifications,
17 sheets of drawings

This certificate of mailing and return receipt postcard in accordance with MPEP 503

☐ Check No. _____ or ☑ credit card charge authorization for **$80.00**

Pancharatnam-Berry phase optical elements with subwavelength gratings

Field of the Invention

The present invention relates to optical elements. More particularly it relates to Pancharatnam-Berry phase optical elements with subwavelength gratings.

Brief Description of the Drawings

Figure 1: Illustration of the principle of PBOEs by use of the Poincare sphere.

Figure 2: The geometry of the space-variant subwavelength grating , as well as the DGPs for incident $|R\rangle$ and $|L\rangle$ polarizations.

Figure 3: Measurements of the transmitted far-field for the subwavelength grating PBOE, when the retardation is $\phi=\pi/2$ and $\phi=\pi$ respectively, for incident (a) circular left, (b) circular right and (c) linear polarizations.

Figure 4: Illustration of the concept of polarization diffraction gratings fabricated using subwavelength quasi-periodic structures. The orientation of the subwavelength grooves, $\theta(x)$, varies periodically in the x-direction, resulting in an element with effective birefringence, whose optical axes (marked by the dark and light arrows in the picture), rotate periodically. The polarization diffraction grating has period d, which is larger than the incident wavelength, λ, whereas the local subwavelength period is $\Lambda < \lambda$. The local optical axes at each point are oriented parallel and perpendicular to the subwavelength grooves.

Figure 5: A diagram describing the operation of polarization diffraction gratings. A beam with polarization $|\mathbf{E}_{in}\rangle$ is incident on the polarization grating. The resulting beam comprises three polarization orders, the EPO, which maintains the original polarization and does not undergo phase modification. The RPO that is $|\mathbf{R}\rangle$ polarized, and whose phase is modified by $2\theta(x)$, and the LPO that is $|\mathbf{L}\rangle$ polarized, and whose phase is modified by $-2\theta(x)$. Since $\theta(x)$ is periodic, the RPO and the LPO undergo diffraction, resulting in the appearance of discrete diffraction orders.

Figure 6: (a) The magnified geometric representation of the continuous blazed polarization diffraction grating; (b) the resulting DGPs for the RPO and LPO formed by this structure. (c) shows a magnified image of a region on the subwavelength structure, demonstrating the local subwavelength period $\Lambda(x,y)$, the local subwavelength groove orientation $\theta(x,y)$, and the local subwavelength grating vector $\mathbf{K}_g$. (d) Scanning electron microscope image of the GaAs dielectric structure.

Figure 7: Images and experimental (dots) and calculated cross-section (solid curves) of the far-field of the beam transmitted through the blazed polarization diffraction gratings, when the incident beam has $|\mathbf{L}\rangle$ polarization, when the incident beam has $|\mathbf{R}\rangle$ polarization, and when the incident beam has linear polarization $|\uparrow\rangle$.

Figure 8: Measurements and predicted diffraction efficiencies in the 1st, -1st and 0 orders of the metal-stripe and dielectric blazed polarization gratings for various incident polarizations. The different incident polarization were achieved by rotating a quarter waveplate (QWP) in front of the linearly polarized light emitted from the CO_2 laser. The graphs show the

efficiencies as a function of the orientation of the QWP. The efficiencies are normalized relative to the total transmitted intensity for each grating.

Figure 9: geometric representation of the subwavelength structure of the binary polarization diffraction grtaing (middle), as well as the DGP that results from this structure (top). The pictures at the bottom are Scanning Electron Microscope images of the dielectric subwavelength structure.

Figure 10: Measured intensity and polarization in the various diffraction orders of the binary polarization diffraction grating for incident (a) $|\mathbf{L}\rangle$ polarization, (b) incident $|\mathbf{R}\rangle$ polarization and (c) incident $|\uparrow\rangle$ polarization, as well as the intensity transmitted through a combination of the binary diffraction grating and a circular polarizer oriented to transmit $|\mathbf{R}\rangle$ polarization for (d) incident $|\mathbf{L}\rangle$ polarization (e) incident $|\mathbf{R}\rangle$ polarization and (f) incident $|\uparrow\rangle$ polarization. The intensities are normalized so that the maximum intensity in each graph is equal to 1.

Figure 11: The far-field images and calculated and measured cross-sections of the beam transmitted through the circular symmetric polarization mode switching, (a) when the incident polarization is $|\mathbf{L}\rangle$, as well as (b) the image and cross-sections of the transmitted $|\mathbf{L}\rangle$ component, and (c) the image and cross sections of the transmitted $|\mathbf{R}\rangle$ component. Also shown, (bottom), the geometry of the subwavelength quasi-periodic structure as well as the spiral DGP caused by this element.

Figure 12: (a) Illustration of the principle of PBOEs by use of the Poincare sphere; the insets display the different local orientations of subwavelength grooves; (b) illustrates the geometrical definition of the grating vector.

Figure 13: The geometry of the subwavelength gratings for different topological charges, as well as an image of typical grating profile taken with a scanning-electron microscope.

Figure 14: (a) The interferogram measurements of the spiral PBOEs; (b) the corresponding spiral phases for different topological charges.

Figure 15: Experimental far-field images as well as their calculated and measured cross sections for the helical beams with $l = 1-4$

Figure 16: Actual quantized phase $F(\phi_d)$ as a function of the desired phase ϕ_d, as well as the multilevel discrete binary local grating orientation. Inset, a scanning electron microscope image of a region on the subwavelength structure.

Figure 17: The magnified geometry of the grating for $N = 4$, as well as the predicted geometrical quantized phase distribution. Also shown, the measured (triangles) and predicted (dashed curve) diffraction efficiency as a function of the number of discrete levels, N.

Figure 18: Illustration of the magnified geometry of a multilevel-PBOE focussing lens with $N = 4$, as well as the predicted multilevel geometrical phase. Inset, the image of the focused spot size as well as the measured (dots), and theoretically calculated (solid curve) cross section.

Detailed Description of Preferred Embodiments

1. Space-variant Pancharatnam-Berry phase optical elements with sub-wavelength gratings:

Space-variant Pancharatnam-Berry phase optical elements based on computer generated subwavelength gratings are presented. By continuously controlling the local orientation and period of the grating any desired phase element can be achieved. We present a

theoretical analysis, and experimentally demonstrate a Pancharatnam-Berry phase based diffraction grating for laser radiation at a wavelength of 10.6 μm.

The Pancharatnam-Berry phase is a geometrical phase associated with the polarization of light. When the polarization of a beam traverses a closed loop on the Poincare sphere, the final state differs from the initial state by a phase factor equal to half the area Ω, encompassed by the loop on the sphere. In a typical experiment, the polarization of a uniformly polarized beam is altered by a series of space-invariant (transversely homogenous) waveplates and polarizers, and the phase, which evolves in the time-domain is measured by means of interference.

Recently, we considered a Pancharatnam-Berry phase in the space-domain. Using space-variant (transversely inhomogeneous) metal stripe subwavelength gratings, we demonstrated conversion of circular polarization into radial polarization, and showed that the conversion was accompanied by a space-variant phase modification of geometrical origin that effected the propagation of the beams. Previously Bhandari suggested using a discontinuous spatially varying waveplate as a lens based on similar geometrical phase effects. Recent studies have investigated periodic polarization gratings. These authors showed that the polarization of the diffracted orders could differ from the polarization of the incident beam. We intend to prove and utilize a connection between the properties of such polarization gratings and the space-domain Pancharatnam-Berry phase.

In this paper we consider optical phase elements based on the space-domain Pancharatnam-Berry phase. Unlike diffractive and refractive elements, the phase is not introduced through optical path differences, but results from the geometrical phase that accompanies space-variant polarization manipulation. The elements are polarization

dependent, thereby enabling multi-purpose optical elements, suitable for applications such as optical switching, optical interconnects and beam splitting. We show that such elements can be realized using continuous computer-generated space-variant subwavelength dielectric gratings. The continuity of the gratings ensures the continuity of the resulting field thereby eliminating diffraction associated with discontinuities, and enabling the fabrication of elements with high diffraction efficiency. We experimentally demonstrate Pancharatnam-Berry phase diffraction gratings for CO_2 laser radiation at a wavelength of $10.6\mu m$, showing an ability to form complex polarization-dependent continuous phase elements.

Figure 1 illustrates the concept of Pancharatnam-Berry phase optical elements (PBOEs) on the Poincare sphere. Circularly polarized light is incident on a waveplate with constant retardation and a continuously space varying fast axis whose orientation is denoted by $\theta(x,y)$. We will show that since the waveplate is space varying, the beam at different points traverses different paths on the Poincare sphere, resulting in a space-variant phase-front modification originating from the Pancharatnam-Berry phase. Our goal is to utilize this space-variant geometrical phase to form novel optical elements.

It is convenient to describe PBOEs using Jones calculus. In this formalism, a waveplate with a space-varying fast axis, is described by the operator, $\mathbf{T}(x,y) = \mathbf{R}(\theta(x,y))\mathbf{J}(\phi)\mathbf{R}^{-1}(\theta(x,y))$, where $\mathbf{J}(\phi)$ is the operator for a waveplate with retardation ϕ, $\mathbf{R}$ is the operator for an optical rotator and θ is the local orientation of the axis at each point (x,y). For simplicity, we work with the helicity basis in which $|L\rangle$ denotes left-hand circular polarization, and $|R\rangle$ denotes right-hand circular polarization. In this

representation, $\mathbf{T}(x,y)$ has the explicit form,

$$\mathbf{T}(x,y)=\cos(\phi/2)\begin{bmatrix}1 & 0\\ 0 & 1\end{bmatrix}-i\sin(\phi/2)\begin{bmatrix}0 & \exp(i2\theta(x,y))\\ \exp(-i2\theta(x,y)) & 0\end{bmatrix}. \qquad (1)$$

Thus, if a beam with polarization $\mathbf{E}_i$ is incident on $\mathbf{T}(x,y)$, the resulting beam has the explicit form,

$$\mathbf{E}_0=\mathbf{T}(x,y)\mathbf{E}_i=\cos(\phi/2)\mathbf{E}_i-i\sin(\phi/2)\left[\langle\mathbf{E}_i|R\rangle\exp(-i2\theta)|L\rangle+\langle\mathbf{E}_i|L\rangle\exp(i2\theta)|R\rangle\right]. \quad (2)$$

Using Eq. (2) we can calculate the Pancharatnam phase-front of the resulting wave. We define this phase-front based on Pancharatnam's definition for the phase between two beams of different polarization as $\varphi_p(x,y)=\arg\left[\langle\mathbf{E}_0(0,0)|\mathbf{E}_0(x,y)\rangle\right]$. This calculation yields that for incident $|R\rangle$ polarization, $\varphi_p(x,y)=-\theta+\arctan[\cos\phi\tan\theta]=-\theta+\arctan[\sin(2\chi)\tan\theta]$, where χ is the ellipticity of the resulting beam. Geometrical calculations show that φ_p is equal to half the area of the geodesic triangle, Ω on the Poincare sphere defined by the pole $|R\rangle$, $|\mathbf{E}_0(0)\rangle$ and $|\mathbf{E}_0(\theta)\rangle$, as illustrated in Fig. 1, yielding the expected Pancharatnam-Berry phase. Similar results can be found for any incident polarization.

Consequently, if a circularly polarized beam is incident on a space-variant polarization-state manipulator, it is subject to geometrical phase modification. Based on Eq. (2), the resulting wave consists of two components, the zero order, and the diffracted order. The zero order has the same polarization as the original wavefront, and does not undergo any phase modification. On the other hand, the diffracted order has a polarization orthogonal to that of the incoming wave, and it's phase at each point is equal to twice the local orientation of the waveplate, $\theta(x,y)$. Since the phase modification of the wavefront is purely geometrical in origin, the phase of the diffracted orders must also be geometrical. We therefore define the

Diffractive Geometrical Phase (DGP) as the phase of the diffracted orders when the incident beam is circularly polarized. For incident $|R\rangle$ and $|L\rangle$ polarizations the DGP is equal to $-2\theta(x,y)$ and $2\theta(x,y)$ respectively. By correctly determining the local orientation of the waveplate, any desired DGP can be realized, enabling the realization of phase operators such as lenses or diffraction gratings. Furthermore, since the orientation of the waveplate only varies from 0 to π, the DGP is defined modulus 2π, and the elements are analogous to diffractive optical elements. However, unlike diffractive optical elements the phase modification in PBOEs does not result from optical path differences, but from polarization-state manipulation, and is intrinsically polarization dependent, with the transmission function given by the matrix $\mathbf{T}(x,y)$ as defined in Eq. (2). This equation also shows that the diffraction efficiency of the PBOEs depends on the retardation of the waveplate.

A case of special interest is $\phi=\pi$. In this case, we find that the diffraction efficiency is 100%, and that $|R\rangle$ polarization is completely converted into $|L\rangle$ polarization. However, despite the fact that the resulting polarization is space-invariant, The Pancharatnam phase, $\varphi_p = -2\theta(x,y)$, is equal to the DGP. This phase corresponds to half the area encompassed by two geodesic paths between the poles that form an angle of 2θ with one another, as illustrated in Fig. 1. Thus, the DGP is equal to the geometrical Pancharatnam-Berry phase of a PBOE with 100% diffraction efficiency. Note that PBOEs operate in different ways on the two helic polarizations. Consequently, a PBOE lens designed for a wavelength λ, with focal length f,

designed by choosing the direction of the waveplate so that $2\theta(x,y) = \pi r^2/\lambda f\big|_{\mathrm{mod}\,2\pi}$, will be a converging lens for $|R\rangle$ polarization, and a diverging lens for $|L\rangle$ polarization.

PBOEs can be realized using space-variant subwavelength gratings. When the period of the grating is much smaller than the incident wavelength, the grating acts as a uniaxial crystal. Therefore by correctly controlling the depth, structure, and orientation of the grating, the desired PBOE can be made. To design a PBOE, we need to ensure that the direction of the grating stripes, $\theta(x,y)$, is equal to half the desired DGP which we denote as $\varphi_d(x,y)$. Next we define a grating vector $\mathbf{K}_g = K_0(x,y)[\cos(\varphi_d(x,y)/2)\hat{\mathbf{x}} + \sin(\varphi_d(x,y)/2)\hat{\mathbf{y}}]$, where $\hat{\mathbf{x}}$ and $\hat{\mathbf{y}}$ are unit vectors in the x and y direction, $K_0 = 2\pi/\Lambda(x,y)$ is the spatial frequency of the grating (Λ is the local subwavelength period) and $\varphi_d(x,y)/2$ is the space-variant direction of the vector defined so that it is perpendicular to the grating stripes at each point. Next, to ensure the continuity of the grating thereby ensuring the continuity of the resulting optical field, we require $\nabla \times \mathbf{K}_g = 0$, resulting in a differential equation that can be solved to yield the local grating period. The grating function ϕ_g (defined so that $\nabla\phi_g = \mathbf{K}_g$) is then found by integrating $\mathbf{K}_g$ over an arbitrary path.

We designed a PBOE that acts as a diffraction grating by requiring that $\varphi_d = (2\pi/d)x\big|_{\mathrm{mod}\,2\pi}$, where d is the period of the structure. Applying this to the grating vector and solving the equation $\nabla \times \mathbf{K}_g = 0$ yields,

$\mathbf{K}_g = (2\pi/\Lambda_0)\exp-(\pi y/d)[\cos(\pi x/d)\hat{\mathbf{x}} - \sin(\pi x/d)\hat{\mathbf{y}}]$, where Λ_0 is the subwavelength

period at $y=0$. The grating function is then found as $\phi_g(x,y) = (2d/\Lambda_0)\sin(\pi x/d)\exp(-\pi y/d)$. We then realized a Lee-type binary grating describing the grating function, ϕ_g. The grating was fabricated for CO_2 laser radiation with a wavelength of 10.6μm, with $\Lambda_0 = 2\mu m$ and d=2.5mm, and consisted of 12 periods of d. We formed the grating with a maximum local subwavelength period of Λ=3.2μm because the Wood anomaly occurs at 3.24μm for *GaAs*. The grating was realized onto a *500* μm thick *GaAs* wafer using contact printing photolithography and electron-cyclotron resonance etching with BCl_3 to nominal depth of 2.5 μm, to yield a retardation of $\phi = \pi/2$. By combining two such gratings we obtained a grating with retardation $\phi = \pi$. Figure 2 illustrates the geometry of the grating, as well the DGP for incident $|L\rangle$ and $|R\rangle$ polarization states as calculated from Eq. (2). The DGPs resemble blazed gratings with opposite blazed directions for incident $|L\rangle$ and $|R\rangle$ polarization states, as expected from our previous discussions.

Following the fabrication, we illuminated the PBOEs with circular and linear polarization. Figure 3 shows the experimental images of the diffracted fields for the resulting beams, as well as their cross-sections when the retardation was $\phi=\pi/2$ and $\phi=\pi$ respectively. When the incident polarization is circular, and $\phi=\pi/2$, close to 50% of the light is diffracted according to the DGP into the first order (the direction of diffraction depends on the incident polarization), whilst the other 50% remains undiffracted in the zero order as expected from Eq. (2). The polarization of the diffracted order has switched helicity as expected. For $\phi=\pi$, no energy appears in the zero order, and the diffraction efficiency is close to 100%. When the incident polarization is linear $\mathbf{E}_i = 1/\sqrt{2}(|R\rangle + |L\rangle)$, the two helic components of the beam are

subject to different DGPs of opposite sign, and are diffracted to the first orders in different directions. When $\phi=\pi/2$, the zero order maintains the original polarization, in agreement with Eq. (2), whereas for retardation π the diffraction is 100% efficient for both circular polarizations, and no energy is observable in the zero order.

To conclude, we have demonstrated novel polarization-dependent optical elements based on the Pancharatnam-Berry phase. Unlike conventional elements, PBOEs are not based on optical path difference, but on geometrical phase modification resulting from space-variant polarization manipulation.

2. Polarization beam-splitters and optical switches based on space-variant computer generated subwavelength quasi-periodic structures:

Polarization beam-splitters and optical switches based on subwavelength quasi-periodic structures are presented. By locally controlling the orientation and period of the subwavelength grooves, birefringent elements for which the optical axes vary periodically, are realized. We present a theoretical discussion of these elements, as well as a detailed description of the design and realization procedures. We show experimental results for infra-red radiation at a wavelength of 10.6μm.

Polarizing beam-splitters are essential components in polarization-based systems such as ellipsometers, magneto-optic data storage and polarization-based light modulators. Often these applications require that the elements provide high extinction ratios over a wide angular bandwidth while maintaining compact and efficient packaging. Conventional polarizing beam-splitters, employing either natural crystal birefringence or polarization-sensitive

multilayer structures are usually, either cumbersome or sensitive to angular change, and therefore do not fully meet these requirements.

Contemporary research has begun to address the use of polarization diffraction gratings as beam-splitters and optical switches. Unlike scalar diffraction gratings that are based on periodic modification of phase and amplitude, polarization diffraction gratings introduce a periodic spatial change of the state of polarization leading to polarization-dependent diffraction. Furthermore, the polarization of the diffracted orders is generally different from that of the incident beam. Such a device was demonstrated by Davis et al, who used liquid crystals to create a waveplate with space-varying retardation. Alternatively, Gori suggested a grating consisting of a polarizer with a spatially rotating transmission axis and Tervo and Turunen suggested that beam-splitters consisting of spatially rotating wave-plates could be realized using subwavelength gratings. More recently a polarization diffraction grating based on spatially rotating nematic liquid crystals has been demonstrated.

In previous papers we demonstrated space-variant polarization-state manipulations using computer-generated subwavelength structures. When the period of a subwavelength periodic structure is smaller than the incident wavelength, only the zeroth order is a propagating order, and all other orders are evanescent. The subwavelength periodic structure behaves as a uniaxial crystal with the optical axes parallel and perpendicular to the subwavelength grooves. Therefore, by fabricating quasi-periodic subwavelength structures, for which the period and orientation of the subwavelength grooves was space-varying, we realized continuously rotating waveplates and polarizers for CO_2 laser radiation at a wavelength of 10.6μm. Furthermore, we showed that such polarization manipulations necessarily led to phase

modification of geometrical origin, which left a clear signature on the propagation of the resulting wave. The phase introduced did not result from optical path differences but solely from local changes in polarization and was in-fact a manifestation of the geometrical Pancharatnam-Berry phase.

In this paper we present an experimental demonstration of polarization diffraction gratings based on space-variant computer-generated subwavelength structures. We present a novel interpretation of these elements and show that the polarization-related diffraction is indeed connected to the space-varying Pancharatnam-Berry phase mentioned above. We present experimental results for infra-red CO_2 laser radiation that include a polarization diffraction grating based on a space-variant continuous metal-stripe subwavelength structure, a continuously rotating dielectric subwavelength structure and a binary waveplate, for which the direction of the subwavelength grooves varies discretely. We also demonstrate a circular symmetric polarization mode switching based on a computer-generated subwavelength structure, thus enabling alternation between intensity distributions of a bright and dark center.

Figure 4 is a schematic representation of the use of a subwavelength structure as a polarization diffraction grating. The local orientation of the subwavelength grooves, $\theta(x)$, varies linearly in the x-direction, to form a polarization diffraction grating comprising a birefringent element with optical axes (which are parallel and perpendicular to the grating grooves) that rotate periodically in the x-direction. The period of the polarization diffraction grating, d, is larger than the incident wavelength, λ, whereas the local subwavelength period of the grooves, $\Lambda(x,y)$, is smaller than the incident wavelength. When a plane-wave with uniform polarization is incident on such a periodic subwavelength structure, the transmitted

field will be periodic in both polarization and phase, therefore, we can expect this field to yield discrete diffraction orders in the far-field.

It is convenient to describe subwavelength quasi-periodic structures such as the one depicted in Fig. 1 using Jones Calculus. In this representation, a uniform periodic subwavelength structure the grooves of which are oriented along the y-axis can be described by the Jones matrix,

$$\mathbf{J} = \begin{pmatrix} t_x & 0 \\ 0 & t_y e^{i\phi} \end{pmatrix} \quad , \quad (1)$$

where t_x, t_y are the real amplitude transmission coefficients for light polarized perpendicular and parallel to the optical axes and ϕ is the retardation of the grating.

If the orientation of the subwavelength grooves is space-varying, i.e. different at each location, then the subwavelength structure can be described by the space-dependent matrix,

$$\mathbf{T}_C(x) = \mathbf{M}(\theta(x))\mathbf{J}\mathbf{M}^{-1}(\theta(x)) \quad , \quad (2)$$

where θ(x) is the local orientation of the optical axis and $\mathbf{M}(\theta) = \begin{pmatrix} \cos\theta & -\sin\theta \\ \sin\theta & \cos\theta \end{pmatrix}$ is a two–dimensional rotation matrix .

For convenience we adopt the Dirac bra-ket notation, and convert $\mathbf{T}_C(x)$ to the helicity base in which $|\mathbf{R}\rangle = \begin{pmatrix} 1 \\ 0 \end{pmatrix}$ and $|\mathbf{L}\rangle = \begin{pmatrix} 0 \\ 1 \end{pmatrix}$ are the two-dimensional unit vectors for right-hand and left-hand circularly polarized light. In this base, the space-variant polarization operator is

described by the matrix, $\mathbf{T}(x) = \mathbf{U}\mathbf{T}_C\mathbf{U}^{-1}$,where $\mathbf{U} = \frac{1}{\sqrt{2}}\begin{pmatrix} 1 & 1 \\ -i & i \end{pmatrix}$ is a unitary conversion matrix. Explicit calculation of $\mathbf{T}(x)$ yields,

$$\mathbf{T}(x) = \tfrac{1}{2}(t_x + t_y e^{i\phi})\begin{pmatrix} 1 & 0 \\ 0 & 1 \end{pmatrix} + \tfrac{1}{2}(t_x - t_y e^{i\phi})\begin{pmatrix} 0 & \exp[i2\theta(x)] \\ \exp[-i2\theta(x)] & 0 \end{pmatrix}. \quad (3)$$

Thus for an incident plane-wave with arbitrary polarization $|\mathbf{E}_{in}\rangle$ we find that the resulting field is,

$$|\mathbf{E}_{out}\rangle = \sqrt{\eta_E}|\mathbf{E}_{in}\rangle + \sqrt{\eta_R}e^{i2\theta(x,y)}|\mathbf{R}\rangle + \sqrt{\eta_L}e^{-i2\theta(x,y)}|\mathbf{L}\rangle \quad , \quad (4)$$

where $\eta_E = \left|\tfrac{1}{2}(t_x + t_y e^{i\phi})\right|^2$, $\eta_R = \left|\tfrac{1}{2}(t_x - t_y e^{i\phi})\langle\mathbf{E}_{in}|\mathbf{L}\rangle\right|^2$, $\eta_L = \left|\tfrac{1}{2}(t_x - t_y e^{i\phi})\langle\mathbf{E}_{in}|\mathbf{R}\rangle\right|^2$, are the polarization order coupling efficiencies and $\langle\alpha|\beta\rangle$ denotes inner product.

Figure 5 is a graphic representation of the results of Eq. (4). It shows that $|\mathbf{E}_{out}\rangle$ comprises three polarization orders ; the $|\mathbf{E}_{in}\rangle$ polarization order (EPO), the $|\mathbf{R}\rangle$ polarization order (RPO) and the $|\mathbf{L}\rangle$ polarization order (LPO). The EPO maintains the polarization and phase of the incident beam, whereas the phase of the RPO is equal to $2\theta(x)$, and the phase of the LPO is equal to $-2\theta(x)$. We note that the phase modification of the $|\mathbf{R}\rangle$ and the $|\mathbf{L}\rangle$ polarization orders results solely from local changes in polarization and is therefore geometrical in nature. We therefore denote this phase as the Diffractive Geometrical Phase (DGP).

The DGP for the $|\mathbf{R}\rangle$ polarization order is opposite in sign to that of the $|\mathbf{L}\rangle$ polarization order, and if $\theta(x)$ is periodic, the functions $e^{i2\theta(x)}$ and $e^{-i2\theta(x)}$ that appear in Eq. (4) can be

developed into Fourier series. Taking into account the connection between the Fourier series of a function and the Fourier series of its complex conjugate, this leads to the equation,

$$|\mathbf{E}_{out}\rangle = \sqrt{\eta_0}|\mathbf{E}_{in}\rangle + \sqrt{\eta_R}\sum_{m=-\infty}^{\infty} a_m e^{i2\pi mx/d}|\mathbf{R}\rangle + \sqrt{\eta_L}\sum_{m=-\infty}^{\infty} a_{-m}^{*} e^{i2\pi mx/d}|\mathbf{L}\rangle \ , \qquad (5)$$

where $a_m = \frac{1}{2\pi}\int e^{i2\theta(x)} e^{i2\pi mx/d} dx$.

Thus we find that the diffraction efficiency into the m th order of the RPO ($\eta_m^R = |a_m|^2$), is equal to the diffraction efficiency into the –m th order of the LPO ($\eta_{-m}^L = |a_m^*|^2$), and conclude that the RPO and LPO are diffracted in opposite senses.

Based on Eqs. (4-5) we find that there are three degrees of freedom associated with the design of polarization diffraction gratings. The first degree of freedom is the determination of the subwavelength structure parameters, t_x, t_y and ϕ. These parameters determine the amount of energy coupled into the EPO. The second degree of freedom is the grating orientation $\theta(x)$. $\theta(x)$ that determines the DGP, thereby determining the diffraction efficiency into all diffraction orders. The third degree of freedom is the incident polarization $|\mathbf{E}_m\rangle$. It determines the ratio between the energy in the RPO and the energy in the LPO. In the next three sections, we intend to demonstrate how these three degrees of freedom can be utilized for the design and realization of polarization beam-splitters and optical switches using subwavelength quasi-periodic structures.

Supposing we wish to design a blazed polarization diffraction grating, i.e. a grating for which all the diffracted energy is in the 1st order when the incident beam is $|\mathbf{R}\rangle$ polarized. For

$|\mathbf{E}_{in}\rangle = |\mathbf{R}\rangle$ we find that $\eta_R = 0$. Consequently the transmitted beam only consists of the LPO and the EPO. Since the EPO does not undergo any phase modification, all of its energy is located in the zero order, and the only order that contributes energy to the 1st order is the LPO. In order to ensure that all the energy of the LPO will be diffracted into the 1st order, it is required that the DGP for the LPO be equal to $2\pi x/d|_{\text{mod}\,2\pi}$. Consequently, we find that $\theta(x) = -\pi x/d|_{\text{mod}\,\pi}$. Next, in order to ensure that no energy is found in the zero-order, we require that $\eta_L = 0$. This condition leads to the solution $t_x = t_y$ and $\phi = \pi$. Thus by determining the incident polarization, $|\mathbf{E}_{in}\rangle$, the grating orientation, $\theta(x)$, and the grating parameters $t_x = t_y$ and $\phi = \pi$, we are able to create the desired diffraction pattern.

In addition, we note that for such a grating, the DGP for the RPO is $2\theta(x) = -2\pi x/d|_{\text{mod}\,2\pi}$, and therefore if $|\mathbf{E}_{in}\rangle = |\mathbf{L}\rangle$, the grating is blazed in the opposite direction. Thus for arbitrary incident polarization, the diffracted energy will be distributed between the 1st and -1^{st} orders. The distribution is dependent on the polarization of the incident beam. Furthermore, the polarization in the 1st order will always be $|\mathbf{L}\rangle$, and the polarization in the -1^{st} order will always be $|\mathbf{R}\rangle$. Thus, by switching the incident polarization between an $|\mathbf{L}\rangle$ state and an $|\mathbf{R}\rangle$ state, an optical switch can be realized. Furthermore, if we choose $\phi \neq \pi$, then some of the incident energy will be coupled into the EPO, resulting in the appearance of a zero-order that maintains the polarization of the incident beam, thereby demonstrating the usefulness of such a device as a variable polarization-dependent beam splitter.

We now focus our attention on the design of the blazed grating discussed above using a quasi-periodic subwavelength structure. Since the determination of the grating parameters t_x, t_y and ϕ depend mainly on the subwavelength groove profile, and not on the subwavelength groove orientation, we begin by determining the desired subwavelength groove orientation, $\theta(x)$, and period, $\Lambda(x,y)$, for the subwavelength structure with the desired DGP. The grating parameters t_x, t_y and ϕ are later determined by choosing a fabrication process that yields a grating profile with the desired birefringence.

To design a continuous subwavelength structure with the desired DGP, we define a subwavelength grating vector, $\mathbf{K}_g(x,y)$, oriented perpendicular to the desired subwavelength grooves,

$$\mathbf{K}_g(x,y) = K_0(x,y)\cos(\pi x/d)\hat{\mathbf{x}} - K_0(x,y)\sin(\pi x/d)\hat{\mathbf{y}}. \quad (6)$$

$K_0(x,y) = 2\pi/\Lambda(x,y)$ is yet to be determined as the local spatial frequency of the subwavelength structure. Figure 6(c) illustrates this definition of $\mathbf{K}_g(x,y)$. To ensure the continuity of the subwavelength grooves, we require that $\nabla \times \mathbf{K}_g = 0$, leading to the partial differential equation,

$$\frac{\partial K_o}{\partial y}\cos(\pi x/d) + \frac{\partial K_o}{\partial x}\sin(\pi x/d) + \pi/d\, K_0\cos(\pi x/d) = 0 \quad , \quad (7)$$

with the boundary condition $K_0(x,0) = 2\pi/\Lambda_0$, where Λ_0 is the local subwavelength period at y=0. The solution to this problem is given by,

$$\mathbf{K}_g(x,y) = \frac{2\pi}{\Lambda_0}\exp(-\pi y/d)\left[\cos(\pi x/d)\hat{\mathbf{x}} - \sin(\pi x/d)\hat{\mathbf{y}}\right] . \quad (8)$$

Consequently, the grating function is then found by integrating $\mathbf{K}_g$ over an arbitrary path to yield,

$$\phi_g(x,y) = \frac{2d}{\Lambda_0}\sin(\pi x/d)\exp(-\pi y/d) \quad (9)$$

We realized a Lee-type binary subwavelength structure mask described by the grating function of Eq. (9) using high-resolution laser lithography. The amplitude transmission for such a Lee-type binary mask can be derived as,

$$t(x,y) = U_s[\cos(\phi_h) - \cos(\pi q)] , \quad (10)$$

where U_s is the unit step function defined by,

$$U_s(\eta) = \begin{cases} 1, & \eta \geq 0 \\ 0, & \eta < 0 \end{cases} ,$$

and where q is the duty cycle of the grating which was chosen as 0.5. Figure 6 illustrates the geometry of a Lee-type binary subwavelength, as well as the resulting DGPs for the RPO and the LPO formed by this structure. The figure shows a continuous quasi-periodic subwavelength structure with a local subwavelength period $\Lambda(x,y)$ where at each location on the element, the grooves are oriented perpendicular to the required fast-axis, resulting in the desired polarization diffraction grating. The resulting DGPs resemble the phase function of a scalar blazed grating. The RPO is blazed in the opposite direction of the LPO as discussed above. Hence, incident $|\mathbf{R}\rangle$ polarization is diffracted in the opposite direction of incident $|\mathbf{L}\rangle$ polarization. The local subwavelength periodicity gives the structure its birefringence, whilst the continuity of the subwavelength grooves ensures the continuity of the resulting field.

Furthermore, we note the space-varying nature of $\Lambda(x, y)$. This is a necessary result for the requirement of continuity posed on the subwavelength grooves.

We realized three different subwavelength structures with the geometry shown in Fig. 3. The first element was realized as a metal stripe subwavelength structure using contact photolithography and lift-off, and the other two elements were dielectric gratings realized using contact photolithography and dry etching techniques. The elements were realized for CO_2 laser radiation at a wavelength of 10.6μm on 500 μm thick GaAs wafers. We fabricated the gratings with $\Lambda_0 = 2\,\mu m$, and $d = 2.5mm$, consisting of 12 periods of d. The gratings were formed with maximum local subwavelength period of $\Lambda = 3.2\,\mu m$ because the Wood anomaly occurs at $3.24\,\mu m$ for GaAs. The metal stripes consisted of a 10nm adhesion layer of Ti and 60nm Au with a duty cycle of 0.6 yielding measured values of $t_x = 0.6$, $t_y = 0.2$, and $\phi = 0.6\pi$. The dielectric gratings were fabricated using electron-cyclotron resonance etching with BCl_3 to nominal depth of $2.5\,\mu m$ and duty cycle of 0.5, resulting in measured values of a retardation $\phi = \pi/2$, and $t_x = t_y = 0.9$. By combining two such gratings, we obtained a grating with retardation $\phi = \pi$, and $t_x = t_y = 0.89$. These values are close to the theoretical predictions achieved using rigorous coupled wave analysis. Figure 6(d) shows a scanning electron microscope image of one of the dielectric structures. We note the local periodicity of the structure and the clear profile of the subwavelength grooves.

Following the fabrication we illuminated the structures with polarized light. Figure 7 shows images of the far-field intensity distributions of the transmitted beams, as well the measured

and predicted intensity cross-sections for incident $|\mathbf{R}\rangle$ polarization, for incident $|\mathbf{L}\rangle$ polarization and for incident linear polarization ($|\mathbf{E}_m\rangle = |\uparrow\rangle$). There is a good agreement between experiment and theory, which was calculated using Eq. (4), and far-field Fraunhoffer intensities. For incident $|\mathbf{R}\rangle$ polarization only the zero order and the 1st order appear. The zero order is due to the EPO, and maintains the polarization of the incident beam, whereas the 1st order is derived from the LPO and has $|\mathbf{L}\rangle$ polarization. For incident $|\mathbf{L}\rangle$ polarization, the zero-order and the -1^{st} order appear, and the polarization of the -1^{st} order is $|\mathbf{R}\rangle$. In the case of incident linear polarization, we note the linear polarization of the zero order, the $|\mathbf{L}\rangle$ polarization of the 1st order and the $|\mathbf{R}\rangle$ polarization of the -1^{st} order as discussed above. We note that for the grating in which $t_x = t_y = 0.89$ and $\phi = \pi$, $\eta_L = 0$, consequently, all of the energy is diffracted into the 1st and -1^{st} orders, as expected.

Figure 8 shows the predicted and measured diffraction efficiencies for the three blazed polarization diffraction gratings for various incident polarization states. The diffraction efficiencies are normalized relative to the total transmitted intensity. The different polarization-states were achieved by rotating a quarter wave-plate in front of the linearly polarized light emitted from the laser. The experiments agree with the predictions. The diffraction efficiency in the zero-order is equal to η_L. It has a different value for each of the grating, however, for each grating, it remains constant regardless of the incident polarization. On the other hand, the diffraction into the 1st and -1^{st} orders depends on the incident

polarization, illustrating the usefulness of polarization diffraction gratings as variable polarization beam-splitters and light modulators.

To further examine the use of polarization diffraction gratings as beam splitters and optical switches, we fabricated a binary polarization diffraction grating using a subwavelength dielectric structure. Each period, d, $(d > \lambda)$, of the grating is comprised of two regions. The subwavelength grating vector in the first region pointed along the x-axis, and the subwavelength grating vector in the second region pointed along the y-axis. i.e,

$$\theta(x) = \begin{cases} 0 & 0 < x < d/2 \\ \pi/2 & d/2 < x < d \end{cases} \quad . \quad (11)$$

We fabricated the subwavelength structure on a GaAs wafer with $t_x = 0.95$, $t_y = 0.84$, and $\phi = 0.45\pi$. The structure was fabricated with d=200μm and $\Lambda(x, y) = 2\mu m$. Figure 9 shows a schematic representation of the subwavelength structure, a graph depicting the resulting DGP and scanning electron microscope images of the subwavelength structure which we had fabricated. We note that the DGP is the same for both the RPO and the LPO. It resembles a scalar binary π–phase grating. Consequently the diffraction efficiencies for both the RPO and the LPO, will be the same as those of a scalar binary π–phase grating i.e.,

$$\eta_m^R = \eta_m^L = \frac{4\sin^2(m\pi/2)}{(m\pi)^2} \quad . \quad (12)$$

Note that for a binary π–phase grating only the odd orders appear and consequently $\eta_0^L = \eta_0^R = 0$. Furthermore, Eq. (12) yields that $\eta_1^{L,R} = \eta_{-1}^{L,R} = 0.405$, and $\eta_3^{L,R} = \eta_{-3}^{L,R} = 0.045$.

Figure 10 shows the measured diffraction efficiencies when the incident beam has (Figs. 7(a,b)) circular and (Fig. 7(c)) linear polarization, as well as the efficiency when the transmitted beam has passed through a circular polarizer oriented to transmit $|\mathbf{R}\rangle$ polarized light (Figs. 7(d-f)). We note that when the beam does not pass through a circular polarizer, the intensity in the various diffracted orders is not dependent upon the incident polarization, however the polarization-state of the diffracted orders does depend on the incident polarization. We note that the intensity of the diffracted orders on the right is equal to the intensity of the diffracted orders on the left, indicative of symmetrical phase structure of the DGP. Furthermore the ratio between the intensity in the 1st and 3rd orders is $\eta_1 / \eta_3 \approx 9$, in agreement with Eq. (12), providing further verification of the binary π–phase of the DGP. In addition, for incident $|\mathbf{R}\rangle$ polarization, the experimental ratio between the intensities in the zero order and in the 1st order is 3.376. This agrees with the predicted ratio of $\eta_R / (\eta_L \eta_1') = \left[\left| t_x + t_y e^{i\phi} \right|^2 / 0.405 \left| t_x - t_y e^{i\phi} \right|^2 \right]$, as predicted using Eqs. (4, 12).

When a circular polarizer, oriented to transmit only $|\mathbf{R}\rangle$ polarized light is applied to the beam, we notice that for incident $|\mathbf{R}\rangle$ polarization (Fig. 7(e)) only the zero order appears. (this is because $\eta_R = 0$). For incident $|\mathbf{L}\rangle$ polarization (Fig. 7(d)) only the orders other than the zero order appear (this is because the EPO has $|\mathbf{L}\rangle$ polarization), and for incident linear polarization (Fig. (7(f)) all diffracted orders appear (this is due all three orders being linearly polarized). Thus, by placing a polarization modulator such as a liquid crystal cell in front of a

setup, comprising a polarization-diffraction grating and a circular polarizer, an optical switch could be assembled for applications such as optical interconnects in communications.

Until now we have discussed polarization beam splitting and optical switching by use of polarization diffraction gratings. However, sometimes a different geometry is required. Suppose for instance, we wish to create an optical switch that enables switching between an optical circularly symmetric mode with a bright center, and an optical circularly symmetric mode with a dark center. This can be done with a quasi-periodic subwavelength structure for which, $\theta(x,y)=\omega(x,y)+c$, where $\omega=\arctan(y/x)$ is the azimuthal angle, and c is a constant number. The DGP of the RPO for such an element is equal to $2(\omega(x,y)+c)$. Thus the RPO carries a vortex with a topological charge of 2, and therefore it has a dark center. Furthermore, since the EPO does not undergo any phase modification, its topological charge is zero, and it exhibits a bright center. Therefore, if we design a quasi-periodic subwavelength structure with $\theta(x,y)=\omega(x,y)+c$, choose $\phi\neq\pi$, and illuminate it with $|\mathbf{L}\rangle$ polarization, the resulting beam will comprise an $|\mathbf{R}\rangle$ polarized vortex carrying beam with a dark center and an $|\mathbf{L}\rangle$ polarized beam with a bright center. We can switch between the two modes using a circular polarizer.

We realized such a quasi-periodic subwavelength structure on a GaAs wafer, with $\theta(x,y)=\omega(x,y)+\pi/4$, yielding a grating function $\phi_g=(2\pi r_0/\sqrt{2}\Lambda_0)[\ln(r/r_0)-\omega]$, where r is a radial coordinate. We chose $\Lambda_0=2\mu m$ and $r_0=5mm$, so that $5mm<r<8mm$ and $2\mu m<\Lambda<3.2\mu m$, and fabricated a dielectric grating with retardation of $\phi=\pi/2$. Note that

for incident $|\mathbf{L}\rangle$ polarization, the transmitted beam had radial polarization in the near field, and that for incident $|\mathbf{R}\rangle$ polarization, the near field had azimuthal polarization. Figure 11 shows far-field images and the measured and calculated cross-sections of (a) the transmitted beam when the incident polarization is $|\mathbf{L}\rangle$ as well as the far-field image of the (b) $|\mathbf{L}\rangle$ and (c) $|\mathbf{R}\rangle$ components of the beam as obtained with a circular polarizer. Figure 11 also shows the geometry of the subwavelength quasi-periodic structure as well as the DGP caused by this element. We note the clear vortex in the DGP. The dark center of the vortex is evident in the measured results where we note that the $|\mathbf{L}\rangle$ component of the transmitted beam (the EPO), has a bright center without undergoing any phase modification, whereas the $|\mathbf{R}\rangle$ component (RPO) has a dark center, clearly indicative of its topological charge. The results clearly demonstrate the circularly symmetric mode switching, which can be realized using subwavelength periodic structures.

To conclude, we have demonstrated polarization diffraction gratings as polarization-sensitive beam-splitters, as well as optical switches. We have demonstrated that the application of subwavelength quasi-periodic structures, for this purpose, is not limited to optical switches based on linear polarization diffraction gratings, and that more complex designs are possible. The introduction of space- varying geometrical phases through space-variant polarization manipulations, enables new approaches for beam-splitting and the fabrication of novel polarization-sensitive optical elements.

3. Formation of helical beams using Pancharatnam-Berry phase optics elements:

Spiral phase elements with different topological charges based on space-variant Pancharatnam-Berry phase optical elements are presented. Such elements can be realized using continuous computer-generated space-variant subwavelength dielectric gratings. We present a theoretical analysis and experimentally demonstrate spiral geometrical phases for infra-red radiation at a wavelength of $10.6\,\mu m$.

Recent years have witnessed a growing interest in helical beams that are exploited in a variety of applications. These include trapping of atoms and macroscopic particles, transferring of orbital angular momentum to macroscopic objects, rotational frequency shifting, the study of optical vortices, and specialized alignment schemes. Beams with helical (or spiral) wavefronts are described by complex amplitudes $u(r,\omega,) \propto \exp(-il\omega)$, where $r,\omega,$ are the cylindrical coordinates, the radial coordinate and azimuthal angle respectively, and l is the topological charge of the beams. At the center, the phase has a screw dislocation, also called a phase singularity, or optical vortex. Typically, helical beams are formed by manipulating the light after it emerges from a laser by superposition of two orthogonal (non-helical) beams, or by transforming Gaussian beams into helical beams by means of computer-generated holograms, cylindrical lenses and spiral phase elements (SPEs). Alternatively, a helical beam can be generated inside a laser cavity by inserting SPEs into the laser cavity. The common approaches of forming SPE are as refractive or diffractive optical elements using a milling tool, single-stage etching process with a gray-scale mask, or with multistage etching process. Such helical beam formations are generally either cumbersome or suffer from complicated realization, high aberrations, low efficiency, or large and unstable setup.

In this Letter we consider novel spiral phase elements based on the space-domain Pancharatnam-Berry phase. Unlike diffractive and refractive elements, the phase is not introduced through optical path differences, but results from the geometrical phase that accompanies space-variant polarization manipulation. We show that such elements can be realized using continuous computer-generated space-variant subwavelength dielectric gratings. Moreover, we experimentally demonstrate SPEs with different topological charges, based on a Pancharatnam-Berry phase manipulation, with an axial symmetric local subwavelength groove orientation, for CO_2 laser radiation at a wavelength of $10.6\,\mu m$.

Recently, we demonstrated space-variant polarization-state manipulations using computer-generated subwavelength structures. When the period of a subwavelength periodic structure is smaller than the incident wavelength, only zeroth order is a propagating order, and all other orders are evanescent. The subwavelength periodic structure behaves as a uniaxial crystal with the optical axes parallel and perpendicular to the subwavelength grooves. Therefore, by fabricating quasi-periodic subwavelength structures, for which the period and orientation of the subwavelength grooves was space-varying, we realized continuously rotating waveplates. Furthermore, we showed that such polarization manipulations inevitably led to phase modification of geometrical origin results from local polarization manipulation and was in-fact a manifestation of the geometrical Pancharatnam-Berry phase. Optical elements that use this effect to form a desired phase-front are called Pancharatnam-Berry phase optical element (PBOE). The formation of PBOE, in this letter, with spiral geometrical phase, indicates an ability to form complex continuous PBOEs.

The PBOEs are considered as waveplates with constant retardation and continuously space varying fast axes, the orientation of which is denoted by $\theta(r,\omega)$. It is convenient to describe PBOEs using Jones calculus. The space-dependent transmission matrix for the PBOE is given by applying the optical rotator matrix on the Jones matrix of the subwavelength dielectric grating to yield in helical basis,

$$\mathbf{T}(r,\omega)=\tfrac{1}{2}(t_x+t_y e^{i\phi})\begin{pmatrix}1 & 0\\ 0 & 1\end{pmatrix}+\tfrac{1}{2}(t_x-t_y e^{i\phi})\begin{pmatrix}0 & \exp[i2\theta(r,\omega)]\\ \exp[-i2\theta(r,\omega)] & 0\end{pmatrix}, \quad (1)$$

where t_x , t_y are the real amplitude transmission coefficients for light polarized perpendicular and parallel to the optical axes, and ϕ is the retardation of the grating. Thus for an incident plane-wave with arbitrary polarization $|\mathbf{E}_{in}\rangle$ we find that the resulting field is,

$$|\mathbf{E}_{out}\rangle=\sqrt{\eta_E}|\mathbf{E}_{in}\rangle+\sqrt{\eta_R}e^{i2\theta(r,\omega)}|\mathbf{R}\rangle+\sqrt{\eta_L}e^{-i2\theta(r,\omega)}|\mathbf{L}\rangle \quad , \qquad (2)$$

where $\eta_E=\left|\tfrac{1}{2}(t_x+t_y e^{i\phi})\right|^2$, $\eta_R=\left|\tfrac{1}{2}(t_x-t_y e^{i\phi})\langle\mathbf{E}_{in}|\mathbf{L}\rangle\right|^2$, $\eta_L=\left|\tfrac{1}{2}(t_x-t_y e^{i\phi})\langle\mathbf{E}_{in}|\mathbf{R}\rangle\right|^2$, are the polarization order coupling efficiencies , $\langle\alpha|\beta\rangle$ denotes inner product, and $|\mathbf{R}\rangle=(1\quad 0)^T$ and $|\mathbf{L}\rangle=(0\quad 1)^T$ represent the right-hand and left-hand circular polarization components respectively. From Eq. (2) one can see that the emerging beam from a PBOE comprises three polarization orders. The first maintains the original polarization state and phase of the incident beam, the second is right-hand circular polarized and has a phase modification of $2\theta(r,\omega)$, and the third is opposite to the second at polarization hand and at phase modification. Note that the polarization efficiencies depend on the groove shape and material as well as on the polarization state of the incident beam. For the substantial case of $t_x=t_y=1$, *and* $\phi=\pi$ an

incident wave with $|\mathbf{R}\rangle$ polarization is subject to entire polarization state conversion and results in emerging field,

$$|\mathbf{E}_{out}\rangle = e^{-i2\theta(r,\omega)}|\mathbf{L}\rangle. \qquad (3)$$

An important feature of Eq. (3) is that the phase factor depends on the local orientation of the subwavelength grating. This dependence is geometrical in nature and originates solely from local changes in the polarization state of the emerging beam. This can be illustrated using the Poincare sphere, representing a polarization state by three Stokes parameters S_1, S_2 and S_3 as depicted in Fig.1(a). The incident right polarized and the transmitted left polarized waves correspond to the north and the south poles of the sphere, respectively. Since the subwavelength grating is space varying, the beam at different points traverses different paths on the Poincare sphere. For instance, the geodesic lines $\overset{\frown}{A}$ and $\overset{\frown}{B}$ represent different paths for two waves transmitted through element domains of different local orientations $\theta(r,0)$ and $\theta(r,\omega)$. Geometrical calculations show that the phase difference $\varphi_p = -2\theta(r,\omega)$ between states corresponding to $\theta(r,0)$ and $\theta(r,\omega)$ orientations, is equal to half of the area Ω enclosed by the geodesic lines $\overset{\frown}{A}$ and $\overset{\frown}{B}$. This fact is in compliance with the well-known rule, proposed by Pancharatnam, for comparing the phase of two light beams with different polarization, and can be considered as an extension of the mentioned rule into the space-domain.

In order to design a continuous subwavelength structure with the desired phase modification, we define a space-variant subwavelength grating vector $\mathbf{K}_g(r,\omega)$, oriented perpendicular to

the desired subwavelength grooves. Figure 1(b) illustrates this geometrical definition of the grating vector. To design a PBOE with spiral geometrical phase, we need to ensure that the direction of the grating grooves is given by $\theta(r,\omega)=l\omega/2$, where l is the topological charge. Therefore, using Fig. 1(b), the grating vector is given by,

$\mathbf{K}_g(r,\omega)=K_0(r,\omega)\{\cos[(l/2-1)\omega]\hat{r}+\sin[(l/2-1)\omega]\hat{\omega}\}$, where $K_0=2\pi/\Lambda(r,\omega)$ is the local spatial frequency of grating with local period of $\Lambda(r,\omega)$. To ensure the continuity of the subwavelength grooves, we require that $\nabla\times\mathbf{K}_g=0$, resulting in a differential equation that can be solved to yield the local grating period. The solution to this problem yields $K_0(r)=(2\pi/\Lambda_0)(r_0/r)^{1/2}$, where Λ_0 is the local subwavelength period at $r=r_0$. Consequently, the grating function ϕ_g (defined so that $\mathbf{K}_g=\nabla\phi_g$) is then found by integrating $\mathbf{K}_g(r,\omega)$ over an arbitrary path to yield,

$\phi_g(r,\omega)=(2\pi r_0/\Lambda_0)(r_0/r)^{l/2-1}\cos[(l/2-1)\omega]/[l/2-1]$ for $l\neq 2$, and $\phi_g(r,\omega)=(2\pi r_0/\Lambda_0)\ln(r/r_0)$ for $l=2$. We then realized a Lee-type binary grating describing the grating function, ϕ_g, for $l=1,2,3,4$. The grating was fabricated for CO_2 laser radiation with a wavelength of $10.6\mu m$, with $\Lambda_0=2\mu m$, $r_0=4.7mm$, and a maximum radius of $6mm$ resulting in $2\mu m\le\Lambda(r)\le 3.2\mu m$. We formed the grating with a maximum local period of $3.2\mu m$ in order not to exceed the Wood anomaly of GaAs. The magnified geometry of the gratings for different topological charges are presented in Fig. 2. The elements were fabricated on $500\mu m$ thick GaAs wafers using contact photolithography and electron-cyclotron resonance etching with BCl_3 to nominal depth of $2.5\mu m$, resulting in

measured values of retardation $\phi = \pi/2$, and $t_x = t_y = 0.9$. These values are close to the theoretical predictions achieved using rigorous coupled wave analysis. The inset in Fig. 2 shows a scanning electron microscope image of one of the dielectric structures.

Following the fabrication, the spiral PBOEs were illuminated with a right hand circularly polarized beam, $|\mathbf{R}\rangle$, at $10.6\mu m$ wavelength. In order to provide experimental evidence of the resulting spiral phase modification of our PBOEs, we used "self-interferogram" measurement using PBOEs with retardation $\phi = \pi/2$. For such elements the transmitted beam comprises two different polarization orders; $|\mathbf{R}\rangle$ poloarization state, and $|\mathbf{L}\rangle$ with phase modification of $-il\omega$, according to Eq. (2). The near-field intensity distributions of the transmitted beams followed by linear polarizer were then measured. Figure 3(a) shows the interferogram patterns for various spiral PBOEs. The intensity dependence on the azimuthal angle is of the form $I \propto 1+\cos(l\omega)$, whereas the number of the fringes is equal to l, the topological charge of the beam. Figure 3(b) illustrates the phase fronts resulting from the interferometer analysis, indicating spiral phases with different topological charges.

Figure 4 shows the far-field images of the transmitted beams having various topological charges, as well as the measured and theoretically calculated cross sections. We achieved the experimental result by focusing the beam through a lens with a 500-mm focal length followed by a circular polarizer. We used the circular polarizer in order to transmit only the desired $|\mathbf{L}\rangle$ state, and to eliminate the $|\mathbf{R}\rangle$ polarization order that appeared because of the error in the

etched depth of the grating to achieve the desired retardation of $\phi = \pi$. Dark spots can be observed at the center of the far-field images, providing evidence the phase singularity in the center of the helical beams. We found an excellent agreement between theory and experiment, clearly indicating the spiral phases of the beams with different topological charges.

To conclude, we have demonstrated the formation of helical beams using space-variant Pancharatnam-Berry phase optical elements based on computer generated subwavelength dielectric grating. The formation of the spiral phase by PBOE is subject to the control of the local orientation of the grating. This can be performed with a high level of accuracy using an advanced photolithographic process. In contrast, the formation of SPE based on refractive optics, where the phase is influenced by fabrication errors due to inaccuracy of the etched three-dimensional profile. We are currently investigating a photolithographic process to achieve accurate control of the retardation phase to yield only the desired polarization order.

4. Formation of multilevel Pancharatnam-Berry phase diffractive optics using space-variant subwavelength gratings:

Multilevel discrete Pancharatnam-Berry phase diffractive optics using computer-generated space-variant subwavelength dielectric grating is presented. The formation of a multilevel geometrical phase is done by discrete orientation of the local subwavelength grating. We discuss a theoretical analysis and experimentally demonstrate a quantized geometrical blazed phase of polarization diffraction grating, as well as polarization dependent focusing lens for infra-red radiation at wavelength $10.6\mu m$.

One of the most successful and viable outgrowths of holography involves diffractive optical elements (DOE). The DOEs diffract light from a generalized grating structure having nonuniform groove spacing. They can be formed as a thin optical element that provides unique functions and configurations. High diffraction efficiencies for DOEs can be obtained with kinoforms that are constructed as surface relief gratings on some substrate. However, in order to reach a high efficiency, it is necessary to resort to complex fabrication processes that can provide the required accuracies for controlling the graded shape and depth of the surface grooves. Specifically, in one process a single photomask with variable optical density is exploited for controlling the etching rate of the substrate to form the desired graded relief gratings, or using multiple binary photomasks so the graded shape is approximated by multilevel binary steps. Both fabrication processes rely mainly on etching techniques that are difficult to accurately control. As a result, the shape and depth of the grooves can differ from those desired, which leads to reduction of diffraction efficiency and poor repeatability of performance.

In this Letter we consider DOEs based on the space-domain Pancharatnam-Berry phase. Unlike diffractive and refractive elements, the phase is not introduced through optical path differences, but results from the geometric phase that accompanies space-variant polarization manipulation. The elements are polarization dependent, thereby, enabling multipurpose optical elements that are suitable for applications such as optical interconnects, beam splitting, and optical switching. Recently, we have demonstrated continuous Pancharatnam-berry phase optical elements (PBOEs) based on subwavelength grating. However, applying the constraint on the continuity of the grating leads to space varying of the local periodicity. Therefore, in order not to exceed the Wood anomaly, the elements are limited in their dimensions as well as

optical parameters. Moreover, the results of space varying periodicity complicates the optimization of the photolithographic process. In order to overcome these limitations, we show that such elements can be realized with a multilevel discrete binary geometrical phase, using a computer-generated space-variant subwavelength dielectric grating. By multilevel discrete controlling of the local orientation of the grating, having uniform periodicity, we can achieve any desired phase element. We experimentally demonstrate Multilevel Pancharatnam-Berry phase Optical Elements (Multilevel-PBOE) as blazed diffraction grating and diffractive focusing lens, for the 10.6-μm wavelength from a CO_2 laser, and show that high diffraction efficiencies can be attained utilizing single binary computer-generated mask, as well as forming multipurpose polarization dependent optical elements.

The PBOEs are considered as waveplates with constant retardation and space varying fast axes, the orientation of which is denoted by $\theta(x,y)$. It is convenient to form such space varying waveplate using subwavelength grating. When the period of a subwavelength periodic structure is smaller than the incident wavelength, only zero order is a propagating order, and all other orders are evanescent. The subwavelength periodic structure behaves as a uniaxial crystal with the optical axes parallel and perpedicular to the subwavelength grooves. Therefore, by fabricating quasi-periodic subwavelength structures, for which the period and orientation of the subwavelength grooves was space varying, we realized rotating waveplates. Furthermore, we showed that such polarization manipulation inevitably led to phase modification of geometrical origin results from local polarization manipulation and was in-fact a manifestation of the geometrical Pancharatnam-Berry phase.

It is convenient to describe PBOEs using Jones calculus. The space-dependent transmission matrix for PBOE is given by applying the optical rotator matrix on the Jones matrix of the subwavelength dielectric grating to yield in helical basis,

$$\mathbf{T}(r,\omega)=\tfrac{1}{2}(t_x+t_y e^{i\phi})\begin{pmatrix}1 & 0\\ 0 & 1\end{pmatrix}+\tfrac{1}{2}(t_x-t_y e^{i\phi})\begin{pmatrix}0 & \exp[i2\theta(x,y)]\\ \exp[-i2\theta(r,\omega)] & 0\end{pmatrix}, \quad (1)$$

where t_x , t_y are the real amplitude transmission coefficients for light polarized perpendicular and parallel to the optical axes, and ϕ is the retardation of the grating. Thus for an incident plane-wave with arbitrary polarization $|\mathbf{E}_{in}\rangle$, we find that the resulting field is,

$$|\mathbf{E}_{out}\rangle=\sqrt{\eta_E}|\mathbf{E}_{in}\rangle+\sqrt{\eta_R}e^{i2\theta(x,y)}|\mathbf{R}\rangle+\sqrt{\eta_L}e^{-i2\theta(x,y)}|\mathbf{L}\rangle \quad , \qquad (2)$$

where $\eta_E=\left|\tfrac{1}{2}(t_x+t_y e^{i\phi})\right|^2$, $\eta_R=\left|\tfrac{1}{2}(t_x-t_y e^{i\phi})\langle\mathbf{E}_{in}|\mathbf{L}\rangle\right|^2$, $\eta_L=\left|\tfrac{1}{2}(t_x-t_y e^{i\phi})\langle\mathbf{E}_{in}|\mathbf{R}\rangle\right|^2$, are the polarization order coupling efficiencies , $\langle\alpha|\beta\rangle$ denotes inner product, and $|\mathbf{R}\rangle=(1\quad 0)^T$ and $|\mathbf{L}\rangle=(0\quad 1)^T$ represent the right-hand and left-hand circular polarization components, respectively. From Eq. (2) it is evident that the emerging beam from a PBOE comprises three polarization orders. The first maintains the original polarization state and phase of the incident beam, the second is right-hand circular polarized and has a phase modification of $2\theta(x,y)$, and the third is opposite to the second at polarization hand and at phase modification. Note that the polarization order coupling efficiencies depend on the groove shape and material, as well as on the polarization state of the incident beam. For the substantial case of $t_x=t_y=1$, *and* $\phi=\pi$ an incident wave with $|\mathbf{R}\rangle$ polarization is subject to entire polarization state conversion and results in emerging field,

$$|\mathbf{E}_{out}\rangle = e^{-i2\theta(x,y)}|\mathbf{L}\rangle. \quad (3)$$

An important feature of Eq. (3) is the phase factor $\phi_d(x,y)\big|_{\mathrm{mod}\,2\pi} = -2\theta(x,y)\big|_{\mathrm{mod}\,2\pi}$ that depends on the local orientation of the subwavelength grating. This dependence is geometrical in nature and originates solely from local changes in the polarization state of the emerging beam.

In our approach, the continuous phase function $\phi_d(x,y)$ is approximated with multilevel discrete binary steps leading to formation of PBOE with multilevel discrete binary local grating orientation. In the scalar approximation, an incident wave front is multiplied by the phase function of the multilevel phase element that is described by, $\exp[iF(\phi_d)]$, where ϕ_d is the desired phase and $F(\phi_d)$ is the actual quantized phase. The division of the desired phase ϕ_d to N equal steps is shown in Fig. 16, where the actual quantized phase $F(\phi_d)$ is given as a function of the desired phase. The Fourier expansion of the actual phase front is given by $\exp[iF(\phi_d)] = \sum_l C_l \exp(il\phi_d)$, where C_l is the lth-order coefficient of the Fourier expansion. The diffraction efficiency, η_l, of the lth-diffracted order is given by $\eta_l = |C_l|^2$. Consequently, the diffraction efficiency η_1 for the first diffracted order for such an element is related to the number of discrete levels N by $\eta_1 = [(N/\pi)\sin(\pi/N)]^2$. This equation indicates that for 2,4,8, and 16 phase quantization levels, the diffraction efficiency will be 40.5%, 81.1%, 95.0%, and 98.7%, respectively. The creation of a multilevel-PBOE is done by multilevel discrete orientation of the local subwavelength grating as illustrated in Fig.16.

Supposing we wish to design a blazed polarization diffraction grating, i.e. a grating for which all the diffracted energy is in the 1st order, when the incident beam is $|\mathbf{R}\rangle$ polarized. We designed a multilevel-PBOE that acts as a diffraction grating by requiring that $\phi_d = (2\pi/d)x\big|_{\mathrm{mod}\,2\pi}$, forming the quantized phase function $F(\phi_d)$ depicted in Fig. 16, where d is the period of the diffraction grating. In order to illustrate the effectiveness of our approach, we realized multilevel diffraction gratings with various number of discrete levels, $N = 2,4,8,16,126$. The grating was fabricated for CO_2 laser radiation with a wavelength of $10.6\mu m$, with diffraction grating period $d = 2mm$ and subwavelength grating period $\Lambda = 2\mu m$. The magnified geometry of the gratings for number of discrete levels, $N = 4$, is presented in Fig. 17, as well as their predicted geometrical quantized phase distribution. The elements were fabricated on $500\mu m$ thick GaAs wafers using single binary mask, contact photolithography and electron-cyclotron resonance etching with BCl_3 to nominal depth of $2.5\,\mu m$, resulting in measured values of retardation $\phi = \pi/2$, and $t_x = t_y = 0.9$. By combining two such gratings we obtained a grating with $\phi = \pi$. These values are close to the theoretical predictions achieved using rigorous coupled wave analysis.

Following the fabrication, the multilevel-PBOEs were illuminated with a right- hand circularly polarized beam, $|\mathbf{R}\rangle$, at $10.6\,\mu m$ wavelength. We used the circular polarized in order to transmit only the desired $|\mathbf{L}\rangle$ state, and to eliminate the $|\mathbf{R}\rangle$ polarization order, which appeared because of the error in the etched depth of the grating to achieve the desired retardation of $\phi = \pi$. Figure 17 shows the measured and predicted diffraction efficiency for

first diffracted order for the different multilevel-PBOEs. There is a good agreement between the experimental results and the prediction efficiencies, providing verification of the expected multilevel discrete binary phase.

In addition, we formed a multilevel Pancharatnam-Berry focusing element for a $10.6\mu m$ wavelength, which had a multilevel discrete spherical phase function of $F(\phi_d) = F[(2\pi/\lambda)(x^2 + y^2 + f^2)^{1/2}]$, with $10\,mm$ diameter, focal length $f = 200mm$, and number of discrete levels $N = 8$. Figure 18 illustrates the magnified geometry of a focusing lens based on multilevel-PBOE with $N = 4$, as well as the predicted multilevel geometrical phase. A scanning electron microscope image of a region on the subwavelength structure, which we had fabricated, is shown in the inset of Fig. 16. Diffraction limited focused spot size for $|\mathbf{L}\rangle$ transmitted beam was measured, while illuminating the element with $|\mathbf{R}\rangle$ polarization state, and inserting a circular polarizer. The inset in Fig. 18 shows the image of the focused spot size as well as the measured and theoretically calculated cross section. The measured diffraction efficiency was 95% in agreement with the predicted value. The geometrical phase of the PBOE is polarization dependent, therefore, we experimentally confirmed that our element is a converging lens for incident $|\mathbf{R}\rangle$ state, and a diverging lens for incident $|\mathbf{L}\rangle$ state, as indicated by Eq. (2). Moreover, it is possible to form bifocal lens for PBOE with a retardation phase of $\phi = \pi$ while illuminating with a linear polarization beam, and inserting refractive lens following the PBOE. Trifocal lens can be created for PBOE with a retardation phase of $\phi = \pi/2$ resulting in distinct three different focuses for $|\mathbf{R}\rangle$, linear, and $|\mathbf{L}\rangle$ polarization states.

To conclude, We have demonstrated the formation of multilevel discrete Pancharatnam-Berry phase optical elements using computer-generated space-variant subwavelength dielectric grating. We realized blazed diffraction grating, as well as polarization dependent focusing lens. The introduction of space varying geometrical phases through multilevel-PBOEs, enables new approaches for novel polarization-sensitive optical elements. We are currently investigating a photolithographic process with the purpose of achieving accurate control of the retardation phase to yield only the desired polarization order.

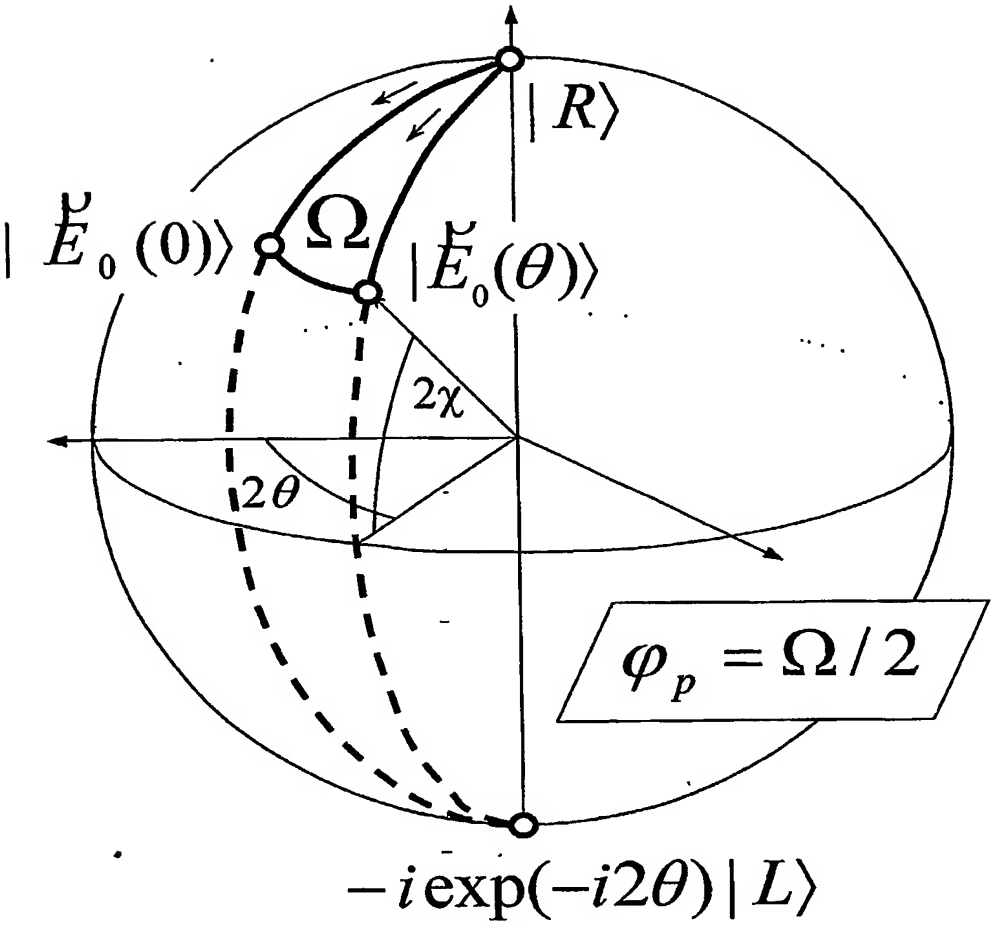
$|R\rangle$
$|\breve{E}_0(0)\rangle$
Ω
$|\breve{E}_0(\theta)\rangle$
2χ
2θ
$\varphi_p = \Omega/2$
$-i\exp(-i2\theta)|L\rangle$

Figure 1

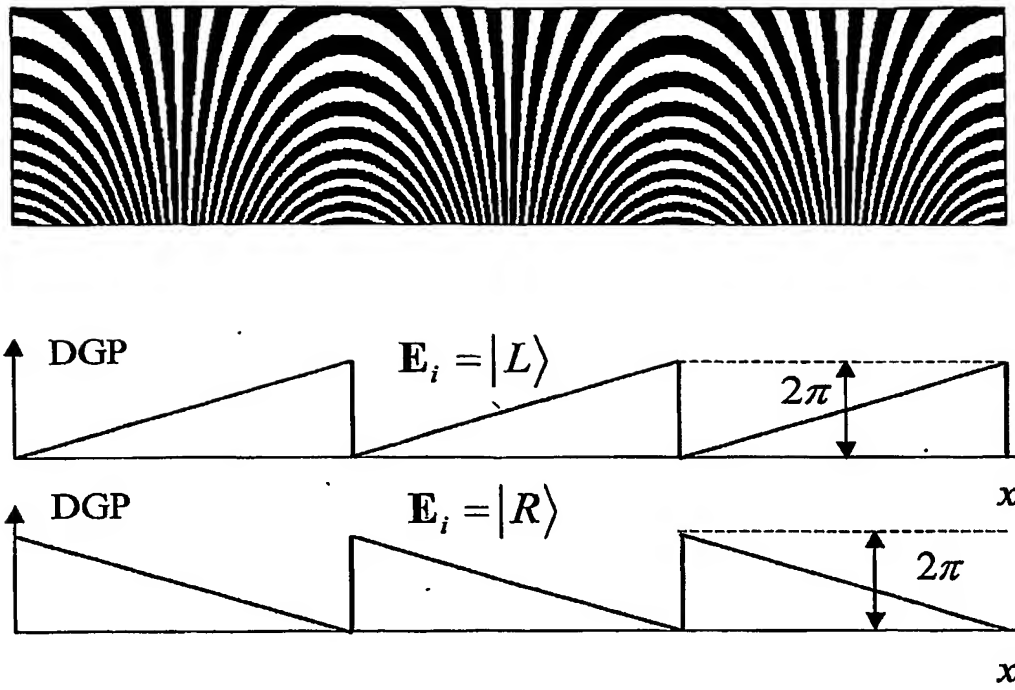

Figure 2

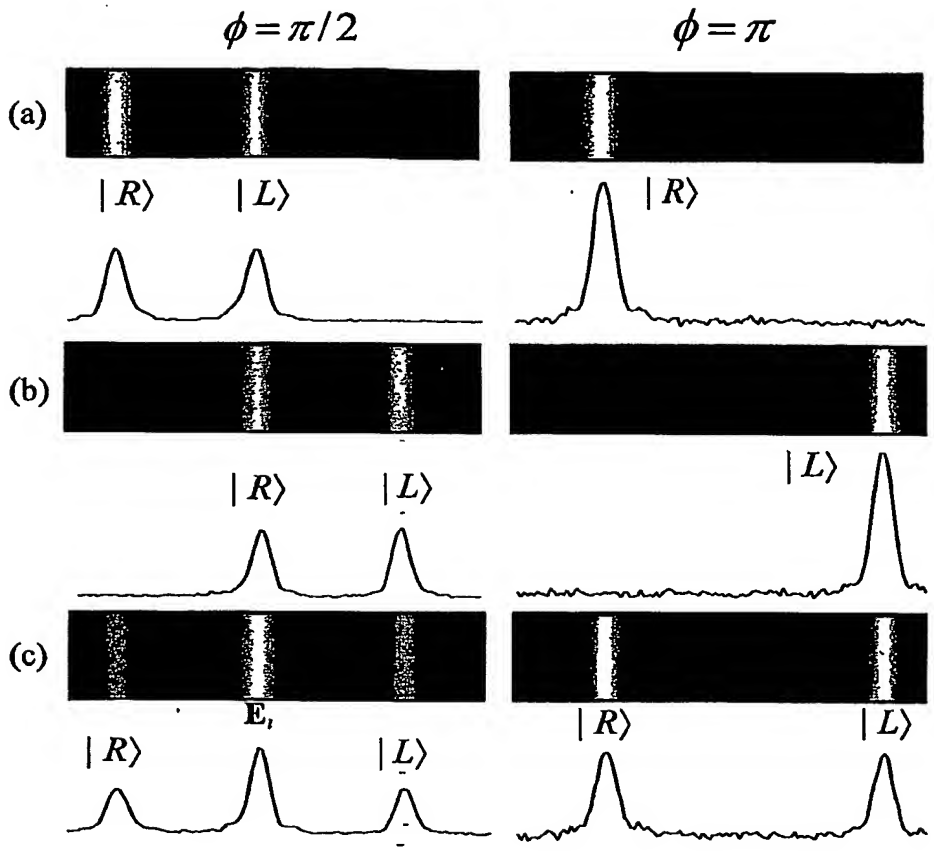
$\phi = \pi/2$
$\phi = \pi$
(a)
$|R\rangle$
$|L\rangle$
$|R\rangle$
(b)
$|R\rangle$
$|L\rangle$
$|L\rangle$
(c)
$\mathbf{E}_t$
$|R\rangle$
$|L\rangle$
$|R\rangle$
$|L\rangle$

Figure 3

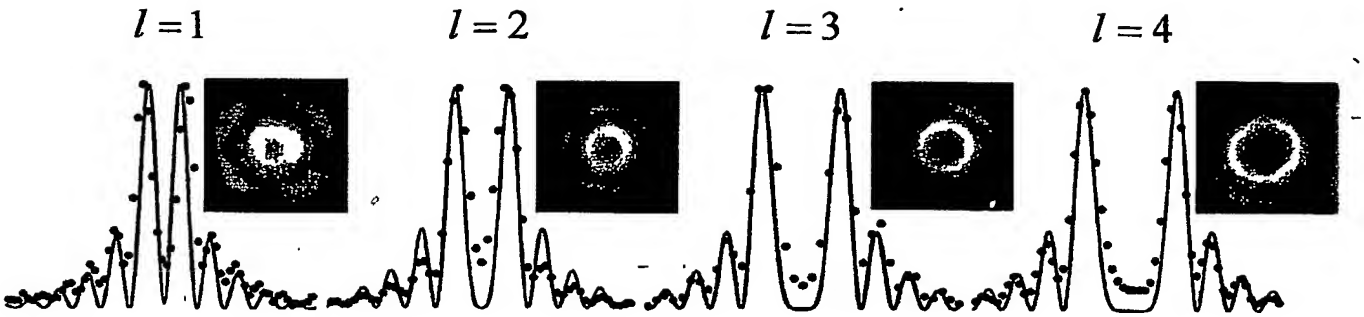

Figure 4

Opt. Lett., Hasman et al.

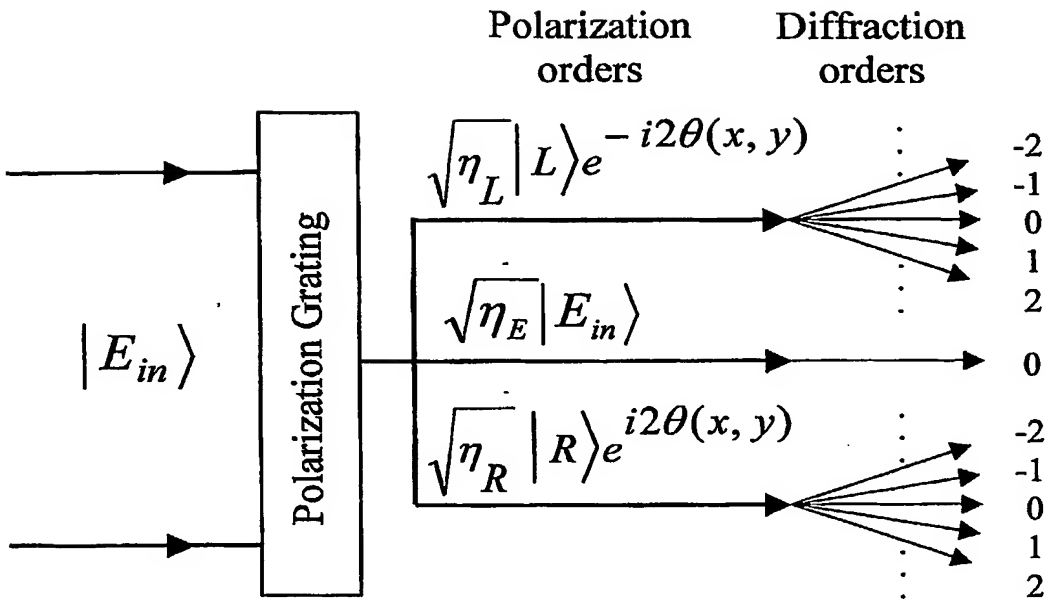
Polarization orders
Diffraction orders
$|E_{in}\rangle$
Polarization Grating
$\sqrt{\eta_L}|L\rangle e^{-i2\theta(x,y)}$
$\sqrt{\eta_E}|E_{in}\rangle$
$\sqrt{\eta_R}|R\rangle e^{i2\theta(x,y)}$
-2
-1
0
1
2
0
-2
-1
0
1
2

Figure 5

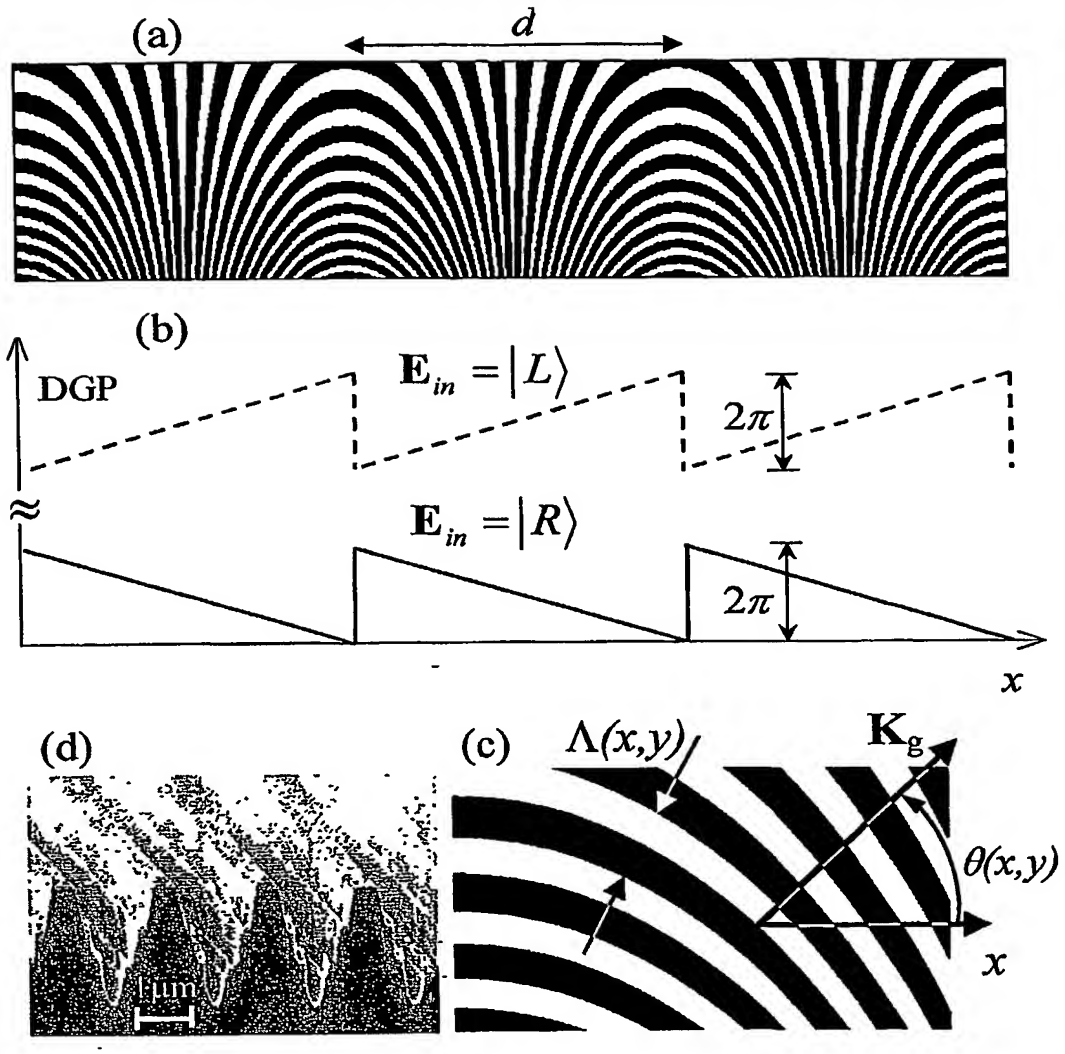
(a)
d
(b)
DGP
$\mathbf{E}_{in} = |L\rangle$
2π
$\mathbf{E}_{in} = |R\rangle$
2π
x
(d)
1μm
(c)
Λ(x,y)
$\mathbf{K}_g$
θ(x,y)
x

Figure 6

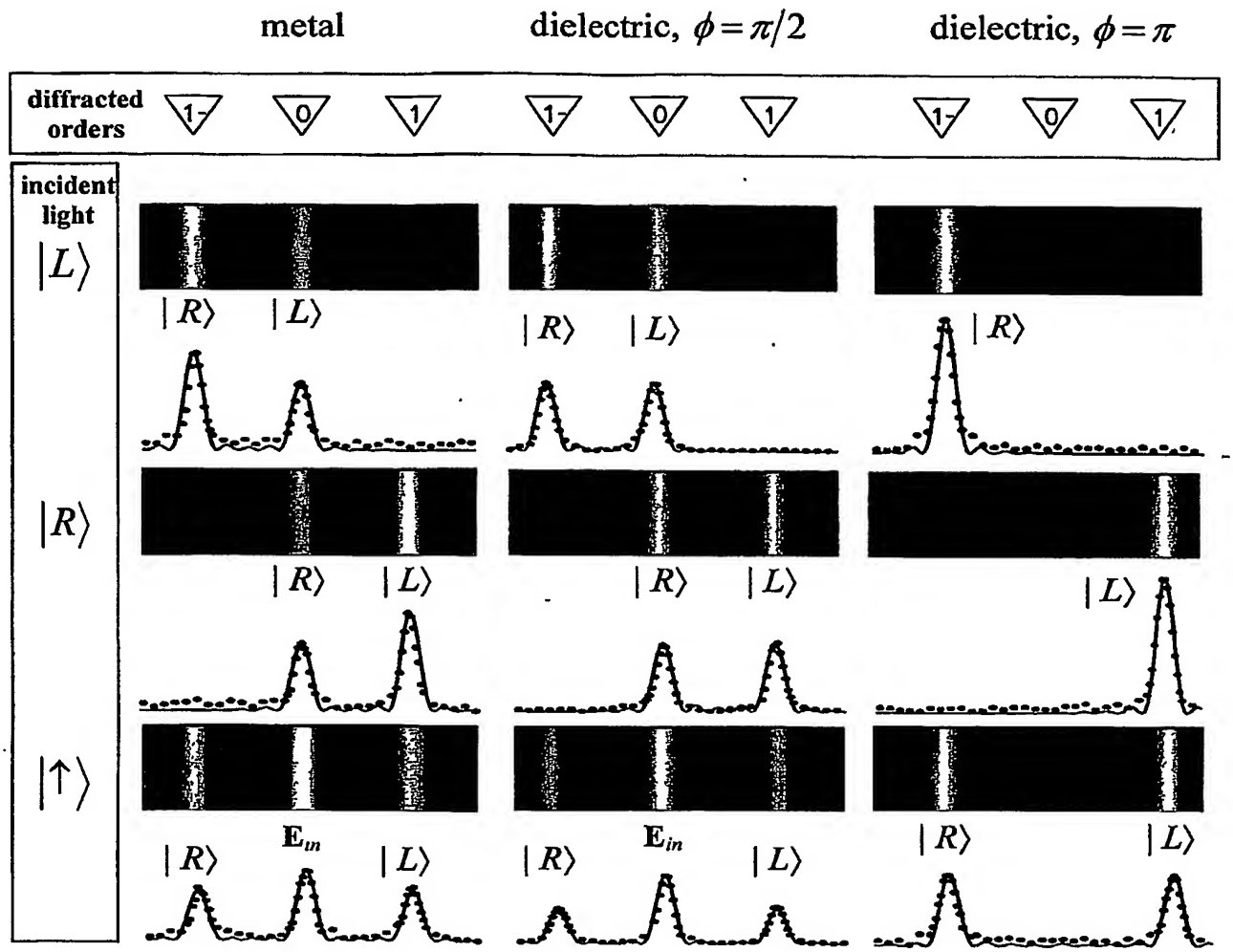
metal
dielectric, $\phi = \pi/2$
dielectric, $\phi = \pi$
diffracted orders
1-
0
1
incident light
$|L\rangle$
$|R\rangle$
$|\uparrow\rangle$
$|R\rangle$ $|L\rangle$
$\mathbf{E}_{in}$

Figure 7

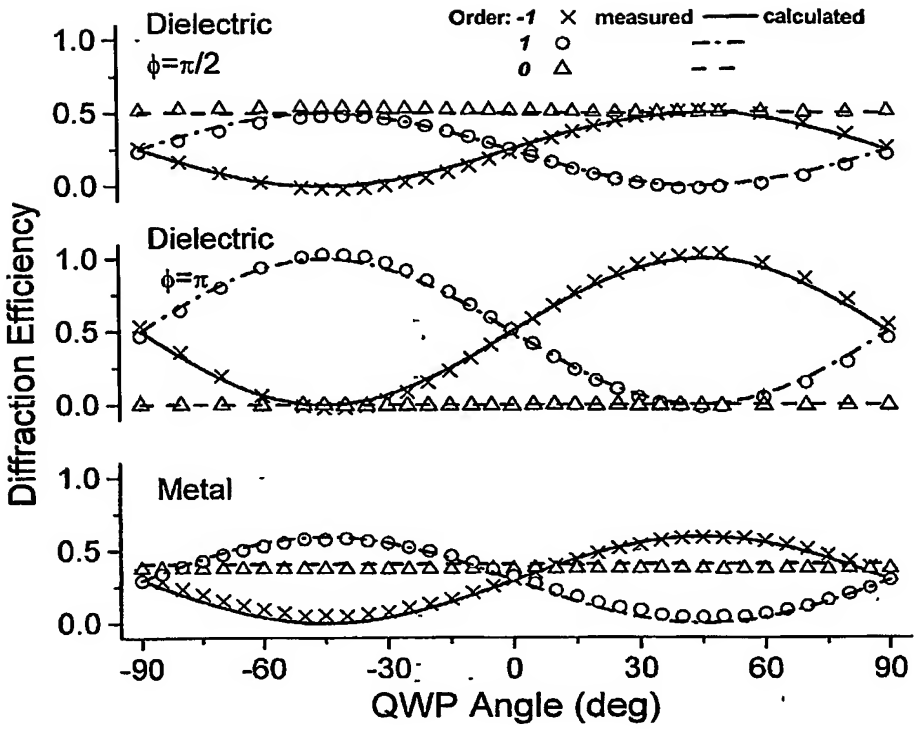
Dielectric
Order: -1 × measured —— calculated
1 ○ -·-
0 △ - -
1.0
ϕ=π/2
0.5
0.0
Dielectric
1.0
ϕ=π
0.5
0.0
Diffraction Efficiency
Metal
1.0
0.5
0.0
-90
-60
-30
0
30
60
90
QWP Angle (deg)

Figure 8

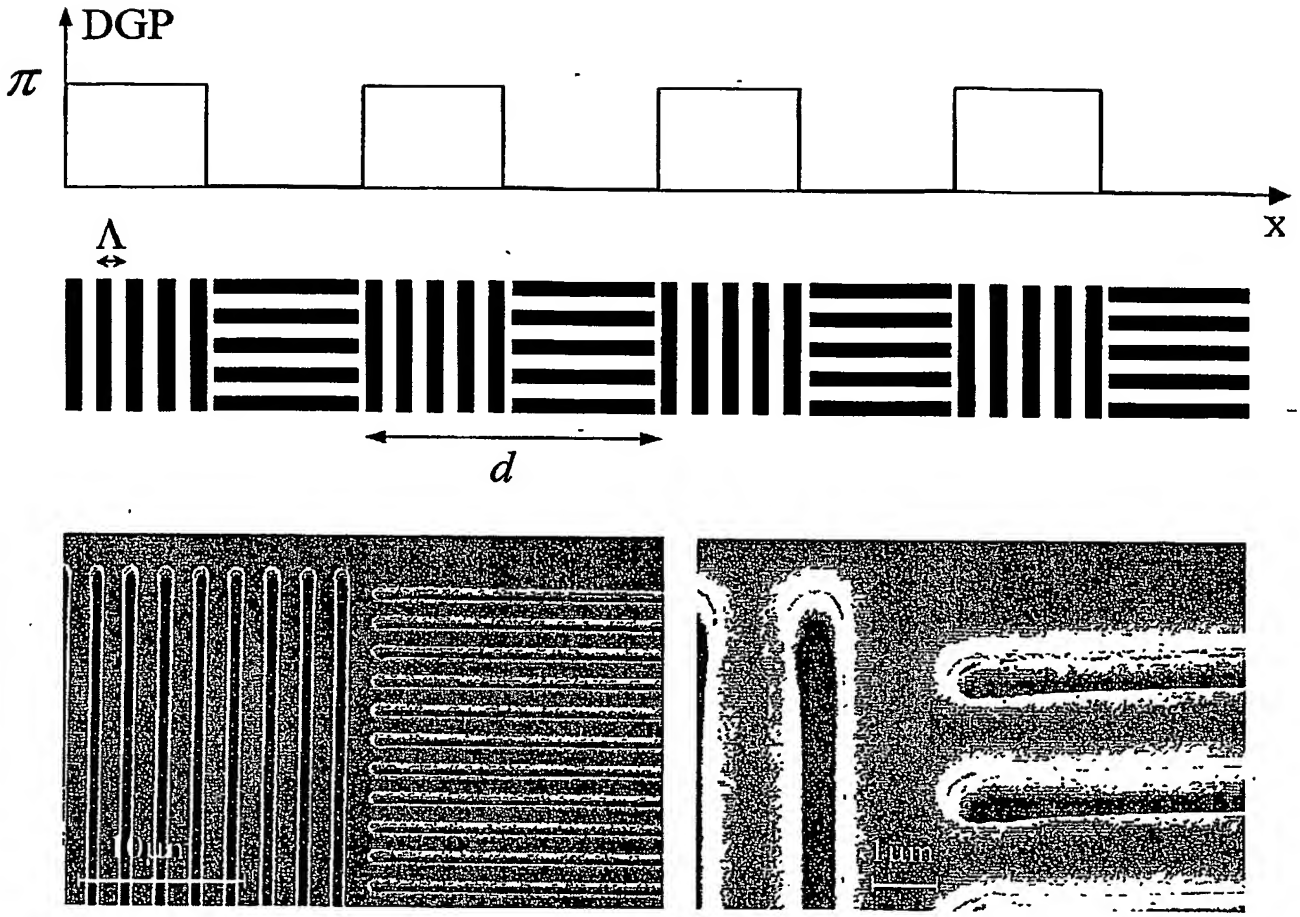

Figure 9

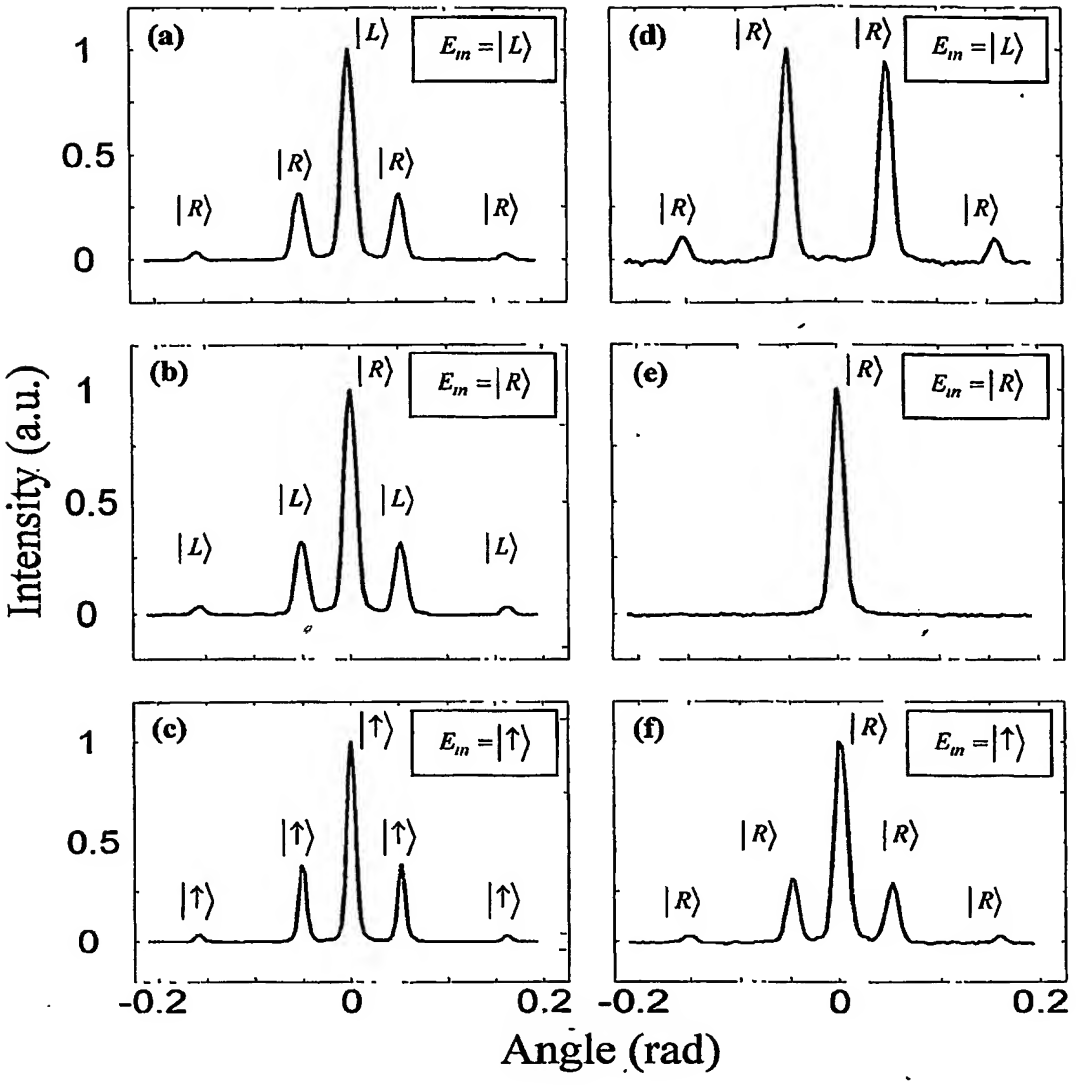
(a)
$E_{in} = |L\rangle$
(d)
$E_{in} = |L\rangle$
(b)
$E_{in} = |R\rangle$
(e)
$E_{in} = |R\rangle$
(c)
$E_{in} = |\uparrow\rangle$
(f)
$E_{in} = |\uparrow\rangle$
Intensity (a.u.)
1
0.5
0
-0.2
0
0.2
Angle (rad)

Figure 10

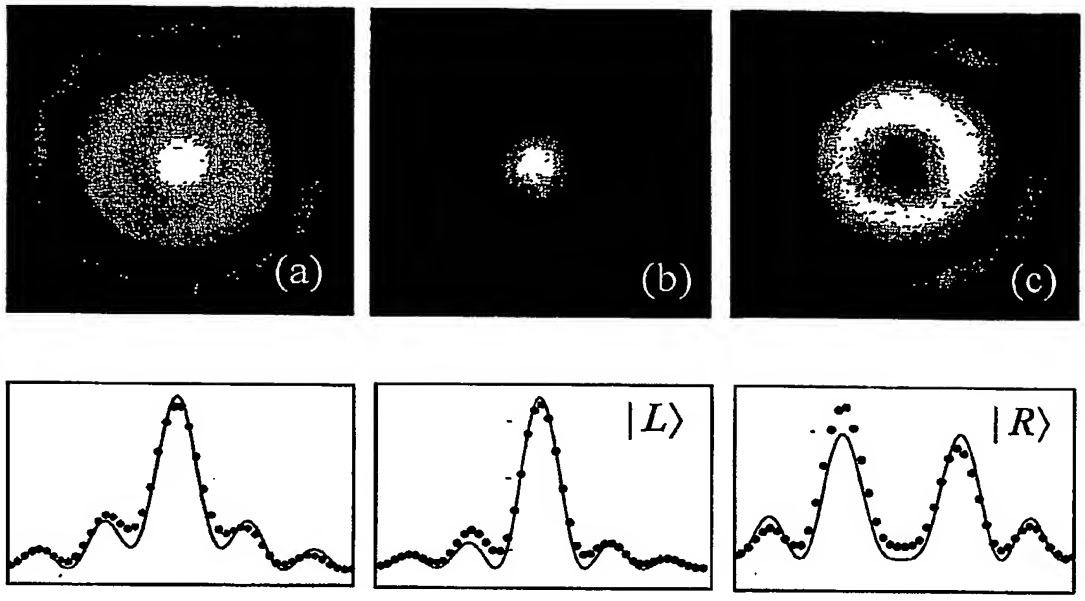

Figure 11

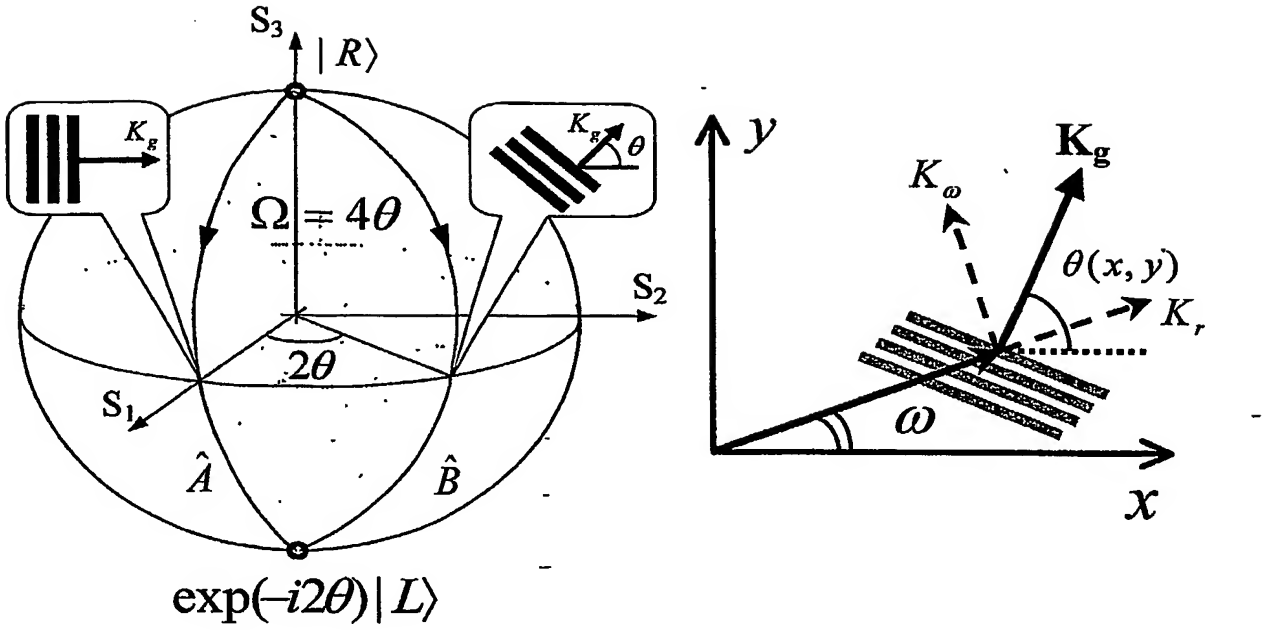

(a) (b)

Figure 12

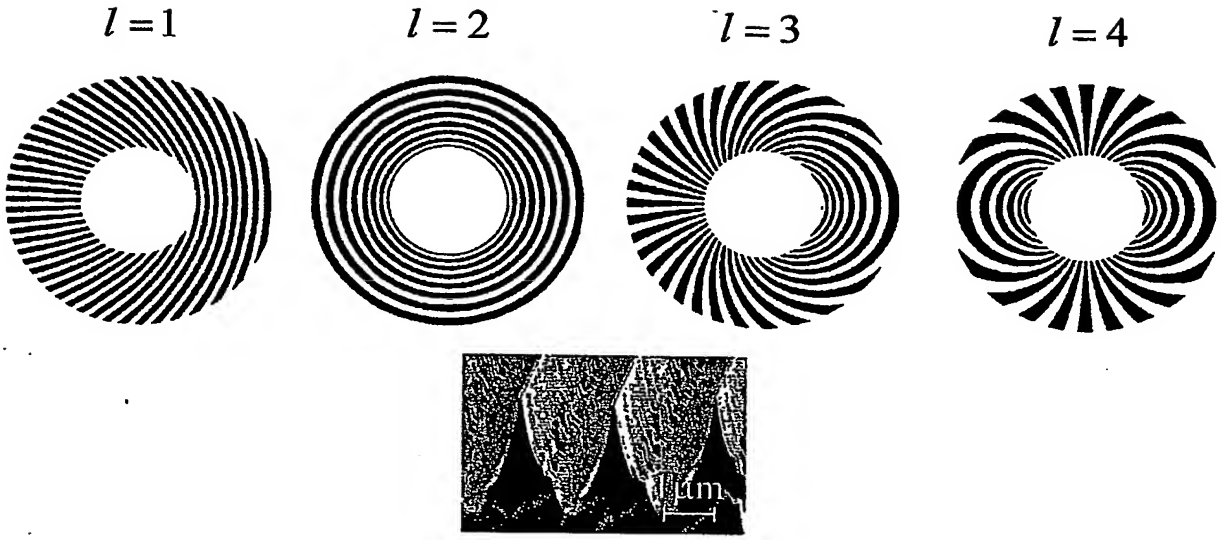

Figure 13

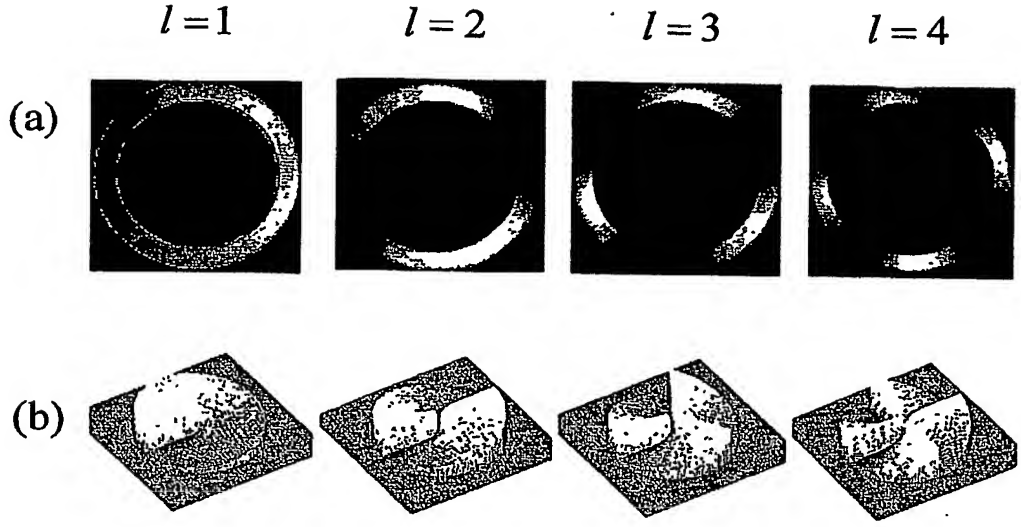

Figure 14

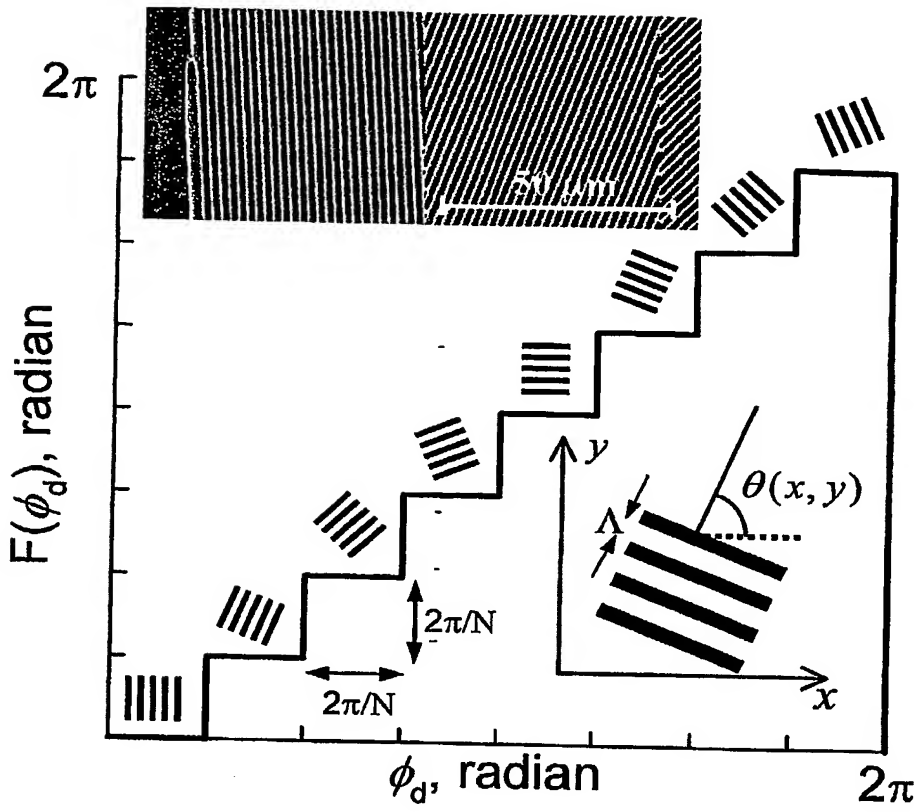

Figure 15

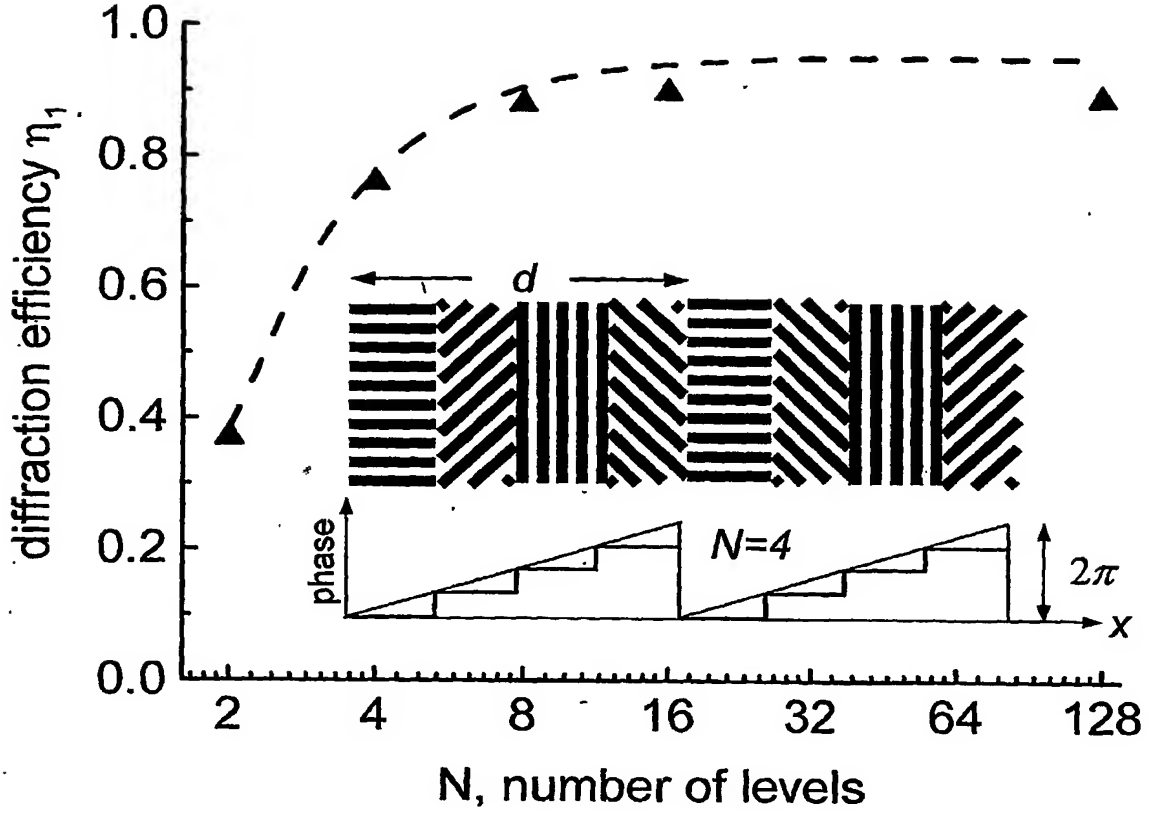
1.0
0.8
0.6
0.4
0.2
0.0
diffraction efficiency η_1
d
phase
N=4
2π
x
2
4
8
16
32
64
128
N, number of levels

Figure 16

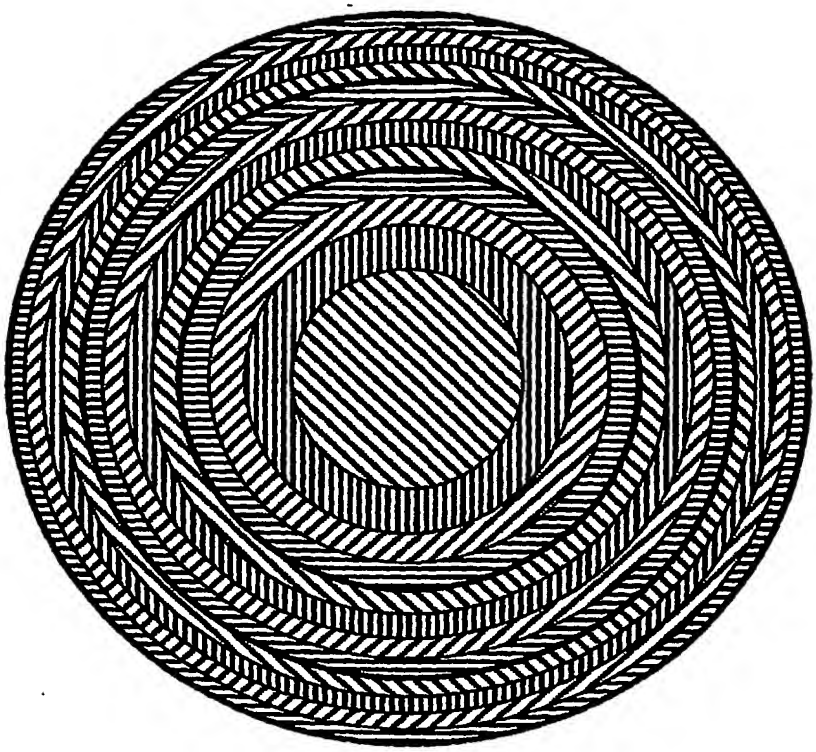

Figure 17

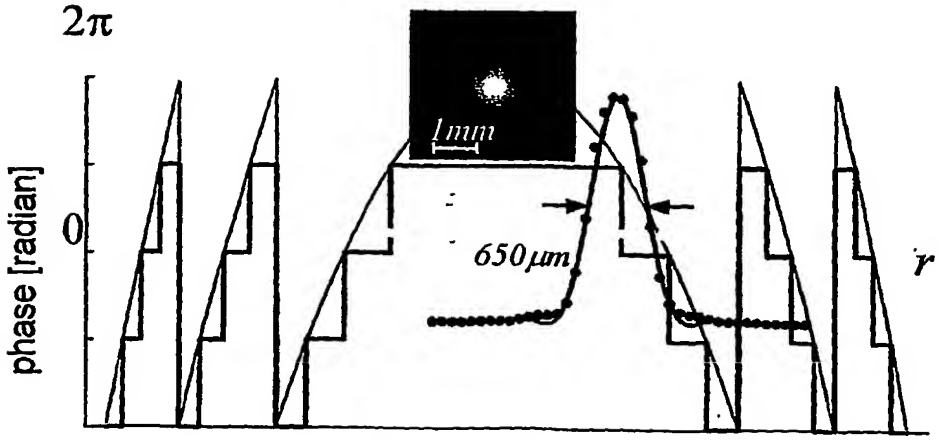

Figure 18